Computers and Electronics in Agriculture 247 (2026) 111612

Contents lists available at ScienceDirect

Computers and Electronics in Agriculture

journal homepage: www.elsevier.com/locate/compag

Original papers

# Performance assessment of no-fee GNSS augmentation systems for tractor guidance

Jaime Gomez-Gil [a,d,*], Angel Alonso-Garcia [a,b], Sergio Alonso-Garcia [a,c], Fco. Javier Gomez-Gil [b,d]

[a] Departamento de Teoría de la Señal, Comunicaciones e Ingeniería Telemática, Universidad de Valladolid, E.T.S.I. de Telecomunicación, Paseo de Belén 15, 47011 Valladolid, Spain
[b] Departamento de Ingeniería Electromecánica, Universidad de Burgos, Escuela Politécnica Superior, Avda. Cantabria s/n, 09006 Burgos, Spain
[c] Empresa TractorDrive, Parque Empresarial La Carpetania, Avenida Leonardo Da Vinci 8, Local B3, 28906 Getafe, Madrid, Spain
[d] Instituto de Neurociencia de Castilla y León, Universidad de Salamanca, Spain

ARTICLE INFO

*Keywords:*
Tractor guidance
GNSS augmentation system
EGNOS
GLIDE
RTK
VRS

ABSTRACT

This study assesses the performance of no-fee GNSS augmentation systems for tractor guidance. Five no-fee augmentation systems: EGNOS, GLIDE, RTK, VRS-NRTK, and on-site RTK were evaluated in both static and guidance tests over short- and long-term periods using three GNSS receiver types: low-cost Navilock NL8022MP, mid-range Novatel Smart2, and high-end Harxon TS108PRO. Static tests recorded 24 h of position data from 14 receiver-augmentation configurations on a fixed surface. Guidance tests recorded trajectory data from the 14 configurations during straight-line guidance using a tractor equipped with two GNSS receivers, one under test and one high-precision reference. Results found that: (i) unaugmented GNSS resulted in guidance errors of 2–3 m, reduced below 1 m in pass-to-pass intervals shorter than 15 min; (ii) EGNOS reduced these guidance errors by ~41%; (iii) GLIDE reduced guidance errors to below 20 cm for pass-to-pass intervals shorter than 15 min, with no long-term improvement; (iv) RTK guidance error decreased as baseline length shortened: >100 km yielded > 17 cm, 20–100 km yielded 3–20 cm, and < 20 km yielded 2–3 cm; (v) VRS-NRTK slightly outperformed RTK with similar baseline lengths; and (vi) on-site RTK enabled 1 cm guidance error. In summary: low-cost receivers without augmentation or with EGNOS result in metre-level errors; mid-range receivers with GLIDE deliver decimetre-level guidance errors in the short term; and high-end receivers using on-site RTK or VRS-NRTK on baselines up to 100 km achieve centimetre-level errors, enabling farmers to replicate tractor trajectories consistently year to year.

## 1. Introduction

GNSS positioning originated with the development of the Global Positioning System (GPS) in the United States and was later expanded through other satellite constellations, including GLONASS, Galileo and BeiDou. GNSS positioning accuracy mainly depends on the receiver type and the augmentation technique employed.

In agricultural applications, two main types of GNSS receivers are commonly used: code receivers, which enable Single Point Positioning (SPP) and typically provide metre-level accuracy (Magiera et al., 2022), and phase receivers, which support Precise Point Positioning (PPP) and/or Real-Time Kinematic (RTK) positioning, achieving centimetre-level accuracy (Alkan et al., 2020).

Augmentation systems provide correction information from reference stations to GNSS receivers and can be broadly classified according to the correction transmission method:

- Unaugmented or autonomous GNSS, mainly used with single-frequency code receivers, delivers metre-level positioning errors in SPP mode (Magiera et al., 2022).
- Satellite-Based Augmentation Systems (SBAS) transmit correction information via satellites. No-fee SBAS services for single-frequency receivers provide modest accuracy improvements.
- Precise Point Positioning (PPP) is a wide-area augmentation technique based on global reference station networks that transmits precise satellite orbit and clock corrections via satellite or the

* Corresponding author at: Departamento de Teoría de la Señal, Comunicaciones e Ingeniería Telemática, Universidad de Valladolid, E.T.S.I. de Telecomunicación, Paseo de Belén 15, 47011 Valladolid, Spain.
*E-mail address:* jgomez@tel.uva.es (J. Gomez-Gil).

https://doi.org/10.1016/j.compag.2026.111612
Received 3 October 2025; Received in revised form 1 February 2026; Accepted 26 February 2026
0168-1699/© 2026 The Author(s). Published by Elsevier B.V. This is an open access article under the CC BY license (http://creativecommons.org/licenses/by/4.0/).

Internet. Commercial agricultural PPP services, such as StarFire (John Deere) and RTX (Trimble), provide decimetre- to centimetre-level positioning accuracy without requiring a local reference station.

- Internet-based augmentation, implemented through Single-Base RTK (SB-RTK) or Network RTK (NRTK), transmits corrections in RTCM format via the Internet and typically provides centimetre-level positioning accuracy (Garrido-Carretero et al., 2019). The availability of NRTK services is commonly documented through Ntrip-list, a publicly accessible directory that catalogues NTRIP casters and mountpoints worldwide, indicating whether correction services are provided free of charge or by subscription, as well as their geographic coverage (Ntrip-list, 2025).
- Radio-based augmentation, based on a local reference station transmitting RTCM corrections via radio, delivers the highest positioning accuracy, typically at the centimetre level (Shannon et al., 2018).

There are also technologies to increase positioning precision without reference stations. GLIDE, from the company Novatel (Novatel, 2015), and e-Dif, from the company Hemisphere, are two of these technologies. GLIDE and e-Dif are designed to improve the precision of relative positioning, whereas previous augmentation systems are technologies focused on increasing the precision of absolute positioning.

Assisted GNSS guidance of tractors helps tractor drivers to steer using lights or a screen. Assisted GNSS equipment is cheaper than automatic GNSS guidance but offers lower guiding accuracies and less driver comfort. Assisted GNSS guidance typically delivers errors of 20 cm Root Mean Square (RMS) regardless of the GNSS positioning accuracy. Although the positioning may be very precise, for example an RTK with a few centimetres of error positioning, agricultural tasks requiring accuracies greater than 20 cm cannot be performed with assisted guidance systems. Assisted GNSS guidance is more accurate than manual guidance, but less accurate than automatic guidance. Likewise, assisted guidance saves fertiliser and herbicide, although less than automatic guidance.

Tractor guidance accuracy depends both on the type of GNSS receiver used, ranging from low-end to mid-range and high-end equipment, and on the augmentation technology applied. Farmers' accuracy needs vary according to the agricultural task. Operations such as fertiliser or herbicide application can be performed with economical guidance equipment, where the key requirement is precision maintained over a short-term period between consecutive tractor passes, typically a few minutes or tens of minutes. Soil preparation and seeding operations demand higher accuracy, although short-term precision is still the main factor determining performance. In contrast, tasks such as strip-till operations and georeferenced weeding require the highest levels of accuracy in both short- and long-term periods between successive agricultural operations in the same field, which can extend over several months or even up to a year. (Barna et al., 2020; Lange and Peake, 2020). While short-term precision in tractor guidance can be readily assessed through guidance tests, long-term accuracy is costly to measure directly and is therefore commonly inferred from simple static GNSS receiver tests, assuming that the receivers' positioning accuracy serves as a lower-bound estimate of long-term guidance accuracy (Kadeřábek et al., 2021).

Automatic GNSS guidance of tractors is the evolution of assisted GNSS guidance of tractors, and, at the beginning of the century, it was already achieving cm-level precision (Keicher and Seufert, 2000). In addition to a GNSS absolute positioning system, precise GNSS automatic guidance systems require a relative positioning system, such as an Inertial Measurement Unit (IMU), to deal with the rough terrain where the tractors work, operate effectively in sloping areas, and provide more stable guidance (Li et al., 2021). At the beginning of the century, the only positioning technology to achieve a precision of cm in guidance was RTK positioning, whereas recently, NRTK positioning achieves close to this precision, reducing costs, because NRTK, unlike RTK, does not require farmers to place a base station near the tractor. The latest advances in tractor guidance include systems to compensate the lateral deviations of the tractor implement (Sun et al., 2010).

The field of automatic tractor guidance has been the subject of extensive experimental and theoretical research. From the extensive body of research, only a limited subset addresses comparative evaluation of tractor guidance under different augmentation systems, such as the following: (i) Nguyen et al.'s contributions include two complementary studies on guidance accuracy, one focused on static GNSS positioning (Nguyen et al., 2021), and the other on real-time guidance evaluation (Nguyen and Cho, 2023). Despite covering a wide range of receivers, the study was limited to RTK positioning with short to medium baseline distances. (ii) A similar comparative study was carried out by Carballido et al., using two augmentation systems: on-site RTK and RTX (Carballido et al., 2014). (iii) A comparable investigation was conducted by Coyne et al., involving one receiver and three augmentation systems: WAAS, OmniStar, and RTK (Coyne et al., 2003). (iv) Kowalczyk and Hadas also conducted a comparative study on GNSS-based tractor guidance, involving one receiver, focused exclusively on guidance rather than static positioning, and including three augmentation systems: SF1, SF3, and RTK with medium baselines (Kowalczyk and Hadas, 2024), and (v) Pérez-Ruiz et al. also contributed with a comparative evaluation involving five augmentation services: RASANT, EUREF-IP, EGNOS, OmniStar, and RTK. This study was limited to short-term guidance tests and did not assess either static positioning or long-term guidance performance (Pérez-Ruiz et al., 2011).

To the best of the authors' knowledge, no previous research has specifically compared the performance of several GNSS augmentation systems in tractor guidance that do not require fee payment, including NRTK, which is available free of charge in Spain and in several other countries. To address this research gap, this work evaluates and compares tractor guidance with five no-fee GNSS augmentation systems, using three different GNSS receivers representing low-cost, mid-range, and high-end categories, including static and guidance tests, and focusing on short- and long-term performance under realistic agricultural conditions. The study specifically investigates:

- How low-, mid-, and high-end receivers perform in tractor guidance.
- How the five no-fee augmentation systems affect short-term precision and long-term accuracy in tractor guidance.
- How baseline length influences RTK-based tractor guidance.
- Which guidance technologies are appropriate for different farming needs.

## 2. Materials and methods

### 2.1. Materials

#### 2.1.1. Positioning receivers

This study tested the performance of three GNSS receivers:

- **Navilock NL8022MP.** This is a low-cost, code-based GNSS receiver compatible with SBAS. The retail price of this receiver was approximately €140 in Spain in 2024. Fig. 1a shows this receiver. More information about this receiver is available in Appendix A.1.
- **Novatel Smart2.** This is a mid-range, dual-frequency, phase-tracking GNSS receiver compatible with SBAS. This receiver also has a proprietary technology known as GLIDE, which reduces the relative pass-to-pass error in agricultural tasks. The retail price of this receiver was approximately €1000 in Spain in 2024. Fig. 1b shows this receiver. More information about this receiver is available in Appendix A.1.
- **Harxon TS108PRO.** This is a high-end, multi-frequency, RTK-enabled GNSS receiver compatible with SBAS. The retail price of this receiver was approximately €2000 in Spain in 2024. Fig. 1c


a b c

**Fig. 1.** GNSS receivers tested in this study: a) Navilock NL8022MP, b) Novatel Smart2, and c) Harxon TS108PRO.

shows this receiver. More information about this receiver is available in Appendix A.1.

In order to obtain a reference positioning, a Harxon TS103 base was used. The retail price of this receiver was approximately €1500 in Spain in 2024.

#### 2.1.2. Tractor guidance system

This study used a setup composed of a John Deere 6400 tractor and a *TractorDrive* guidance system version 3.4, which includes: (i) a guidance computer (Fig. 2a) and the screen of the guidance computer (Fig. 2b) used to implement automatic guidance of the tractor; (ii) the guidance receiver (Fig. 6a) corresponding to each of the 14 tested configurations, connected to the guidance computer; (iii) a DC R30 Maxon motor (Fig. 2b), connected to the guidance computer, which actuates the tractor steering wheel via a friction wheel; (iv) an InvenSense MPU9250 IMU connected to the guidance computer to acquire angular rate and linear acceleration data; (v) a data logging laptop to record the real trajectory followed by the tractor (Fig. 2b); and (vi) a high-precision reference receiver to track the tractor's trajectory (Fig. 6a).

### 2.2. Methods

#### 2.2.1. No-fee GNSS augmentation systems

The receivers were tested with five GNSS augmentation systems: (i) with satellite augmentation using EGNOS, as the tests were conducted in Europe, where EGNOS is the regional SBAS; (ii) with the Novatel's algorithm GLIDE, which, although not strictly an augmentation system, is considered as such in this study due to its ability to improve positioning performance; (iii) with a RTK augmentation via the Internet, connecting to a single-base station located tens or hundreds of kilometres away; (iv) with NRTK augmentation via the Internet, using the VRS algorithm to generate the corrections from base stations of the network, with the closest stations located tens of kilometres away, referred to in this article as VRS-NRTK; and (v) with on-site RTK, augmented via radio from a base station located less than 1 km away.

GNSS positioning exhibits temporal correlation. Factors such as satellite geometry, atmospheric conditions, and multipath effects vary slowly over time, leading to autocorrelated positioning. To account for this, our study explicitly analyzes short-term and long-term tests.

#### 2.2.2. Configurations under test

Specifically, the following 14 configurations were tested:

- **C1 (Navilock):** The Navilock NL8022MP configured to work autonomously with EGNOS turned *off*.
- **C2 (Navilock|EGNOS):** The Navilock NL8022MP configured with EGNOS turned *on*.
- **C3 (Novatel):** The Novatel Smart2 configured with EGNOS turned *off* and GLIDE turned *off*.
- **C4 (Novatel|EGNOS):** The Novatel Smart2 configured with EGNOS turned *on* and GLIDE turned *off*.
- **C5 (Novatel|EGNOS+GLIDE):** The Novatel Smart2 configured with EGNOS turned *on* and GLIDE turned *on*.
- **C6 (Harxon):** The Harxon TS108PRO configured to work autonomously with EGNOS turned *off*.
- **C7 (Harxon|EGNOS):** The Harxon TS108PRO configured with EGNOS turned *on*.
- **C8 (Harxon|RTK|645km):** The Harxon TS108PRO configured with RTK turned *on* to receive RTK corrections from a single-base reference station in Bolvir, Girona, Spain, 645 km from the receiver, via the Networked Transport of RTCM via Internet Protocol (NTRIP).
- **C9 (Harxon|RTK|296km):** Similar to C8, but with the reference station in Mérida, Badajoz, Spain, 296 km from the receiver.
- **C10 (Harxon|RTK|100km):** Similar to C8, but with the reference station in Aranda de Duero, Burgos, Spain, 100 km from the receiver.

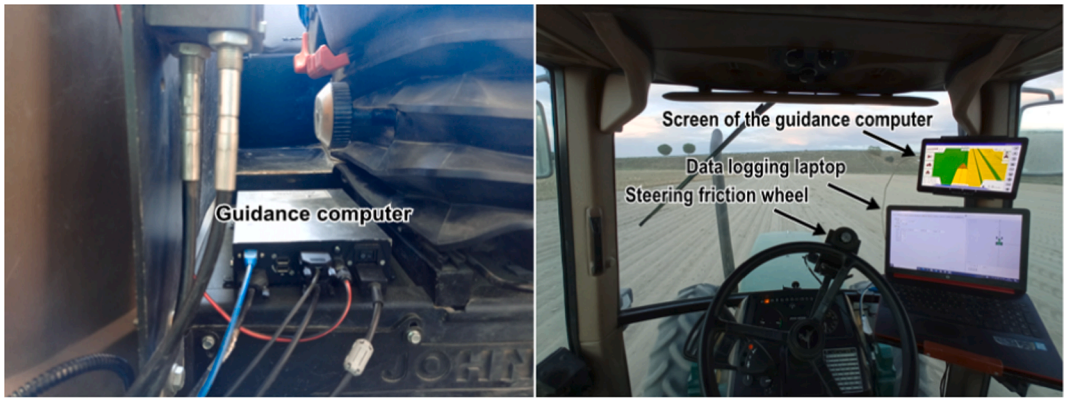


a b

**Fig. 2.** (a) Guidance computer that implements the guidance system. (b) Elements of the experimental setup visible from the tractor operator's position.

- **C11 (Harxon|RTK|42km):** Similar to C8, but with the reference station in Valladolid, Valladolid, Spain, 42 km from the receiver.
- **C12 (Harxon|RTK|14km):** Similar to C8, but with the reference station in Olmedo, Valladolid, Spain, 14 km from the receiver.
- **C13 (Harxon|VRS-NRTK|14,25,42km):** The Harxon TS108PRO configured with RTK turned *on*, to receive RTK corrections from several ERGNSS base stations using the VRS protocol being the receiver located 14, 25 and 42 km from the three nearest reference stations. Augmentation data in this configuration was based on information from these three base stations, although the exact number and identity of contributing base stations cannot be confirmed.
- **C14 (Harxon|On-site RTK):** The Harxon TS108PRO configured with RTK turned *on*, to receive RTK corrections from a Harxon TS103 base station connected by radio to the TS108PRO.

Configurations C8 to C12 used reference stations of the Instituto Geográfico Nacional (IGN) (Ministerio de Transporte y Movilidad Sostenible, 2025), a Spanish public agency that provides RTK corrections via the Internet free of charge throughout Spain. Fig. 3 shows the locations of the IGN reference stations $R_{C8}$ to $R_{C12}$, the virtual reference station used in configuration C13, and the sites where the tests were conducted: static tests took place on a flat platform mounted on a roof in Pozal de Gallinas, Valladolid, Spain, at 41.3178° N, 4.8410° W, and guidance tests took place in a field 1 km from the village, at 41.3051° N, 4.8357° W.

The EGNOS, GLIDE, RTK and VRS-NRTK were activated or deactivated without modifying the default parameters of the receivers. All other configuration parameters remained at the manufacturer's default values, except for the positioning rate, which was set to 5 Hz in all cases.

With the previous fourteen configurations, this study performed (i) **static tests** of the receivers, and (ii) **guidance tests** of a tractor equipped with each receiver. Specifically:

- Static tests were analysed in 15-minute data sets, obtaining short-term static test results, and in 24-hour data sets, obtaining long-term static test results.
- Guidance tests were analysed with data of guidance tests performed in 15 minutes intervals, obtaining short-term guidance test results, and long-term guidance estimations were also obtained.

### 2.2.3. Variables under study

This study computed distance errors in the XY plane, excluding the vertical component. From the positions acquired in each experiment, six statistical error parameters were computed: (i) the RMS error, defined as the square root of the average squared errors and giving greater weight to large errors; (ii) the mean error, defined as the average distance to the reference point; (iii) the Standard Deviation (SD), which quantifies the error dispersion; (iv) the CEP error, defined as the radius of a circle centred on the reference point that contains 50% of the points; (v) the R95 error, corresponding to the radius containing 95% of the points; and (vi) the R99.7 error, which contains 99.7% of the points. These six error parameters were computed for the static tests, while only the first three were calculated for the guidance tests, as the last three are only defined for use in static GNSS tests. All error parameters were computed for both short- and long-term intervals, with short-term errors representing precision and long-term errors representing accuracy.

Tables, figures, and comparisons of results were based on the RMS statistic, as it is the most widely used error metric in autonomous tractor guidance.

Two types of error can be considered in GNSS positioning: relative error, which measures the difference between two GNSS-measured points, and absolute error, which measures the deviation from a real point. Precision, also called repeatability, describes deviation from a mean, while accuracy describes deviation from an absolute position. Terms such as pass-to-pass error or short-term error relate to relative positioning, whereas long-term or year-to-year error relate to absolute positioning (Schaefer and Pearson, 2021). For guidance systems, when the interval between tractor passes is short, typically below 15 minutes, pass-to-pass precision is relevant; for longer intervals, year-to-year precision applies. In this article, **short-term error** refers to relative positioning or guidance over short intervals, and **long-term error** refers to absolute positioning or guidance over longer periods, up to one year.

### 2.2.4. Methodology of static tests

The static tests were performed by placing two Navilock NL8022MP receivers, three Novatel Smart2 receivers, nine Harxon TS108PRO receivers, and one Harxon TS103 base station on a roof with good horizon visibility (Fig. 4a). A laptop computer was connected to the fourteen receivers through a USB hub (Fig. 4b). The laptop, running the Tera Term Windows application, acquired the National Marine Electronics Association (NMEA) 0183 sentences from the fourteen receivers for twenty-four hours on 22 March 2023.

The positions of the RTK receivers in C13 (Harxon VRS-NRTK) and C14 (Harxon on-site RTK) were obtained by averaging the 432,000 points from each receiver, and are referred to as their true positions throughout this article. These reference positions, shown in blue in Fig. 5, were used to determine the true positions of receivers for configurations C1–C12 based on the distances shown in the figure.

Scatter plots in Cartesian coordinates, Cumulative Distribution Functions (CDFs), and graphs of deviation from the initial position over the first 15 minutes were generated.

The RMS, mean, SD, CEP, R95, and R99.7 errors were calculated for static tests over short- and long-term intervals.

For the short term, 96 intervals of 15 minutes were chosen from the

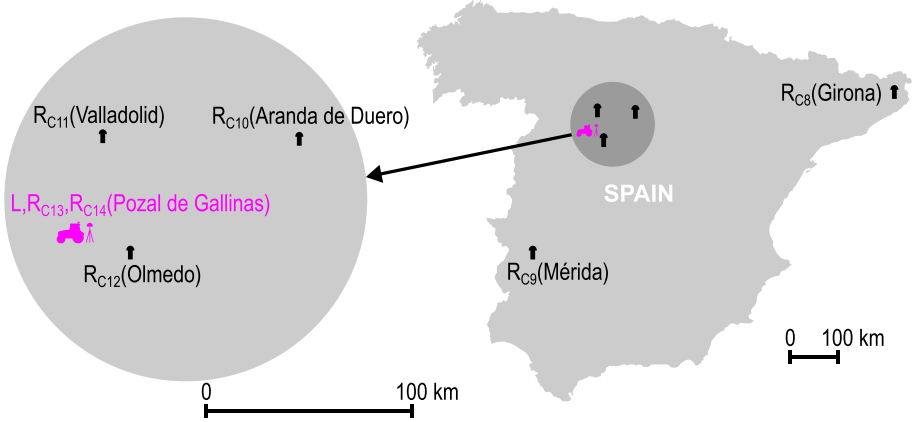


**Fig. 3.** Map that shows some location where the static and guidance tests were performed (L, Pozal de Gallinas, Km 0), and the location of Reference Stations for configurations 8 to 14 ($R_{C8}$–$R_{C14}$).

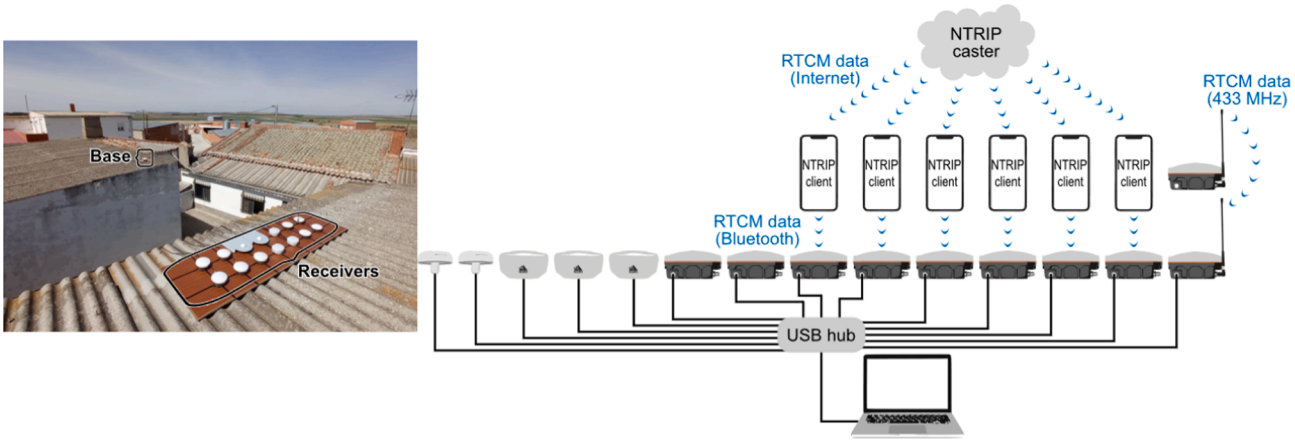


**Fig. 4.** Images of the data acquisition for the static tests: (a) receivers acquiring data on a roof, and (b) diagram of the connection between receivers, base station, and laptop.

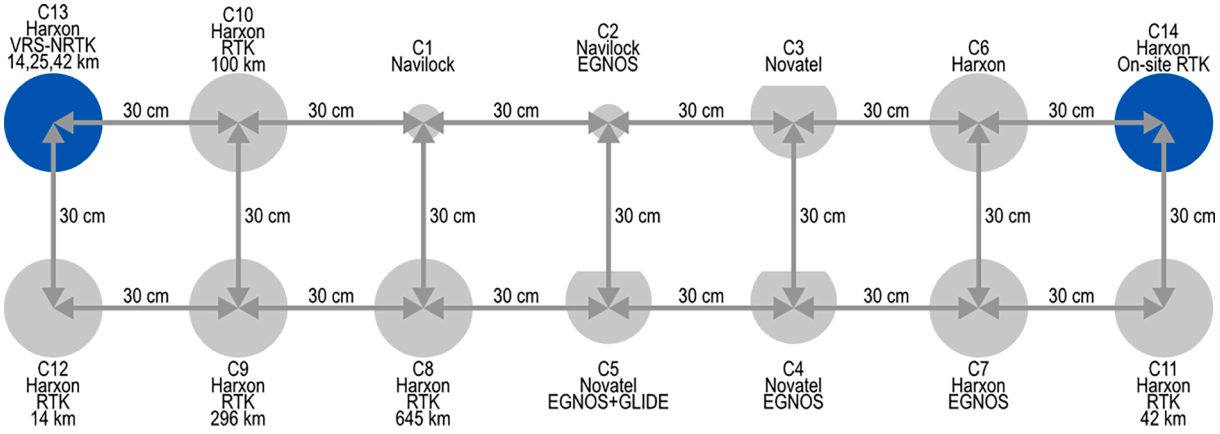


**Fig. 5.** Relative positions of receivers in the static tests. The position of the receivers represented in grey was obtained from the true position computed by receivers in blue, and the distances shown in the figure.

24-hour static test data. The six statistical error parameters were then computed as the mean of each parameter across the 96 intervals. These six means were considered the short-term static error parameters.

For the long term, a single 24-hour interval including all data was chosen. Over this interval, the six statistical error parameters were computed and considered the long-term static error parameters.

### 2.2.5. *Methodology of guidance tests*

The guidance tests were performed with the John Deere 6400 tractor equipped with the tractorDrive autoguidance system, operating with default parameters. The system's IMU was calibrated with the tractor placed on a flat, level surface. Tests were conducted at 1 m/s along a 300 m straight trajectory, employing three GNSS receivers for each configuration (Fig. 6a). The first receiver, referred to in this article as the ***guidance receiver***, was the receiver specified for each of the 14

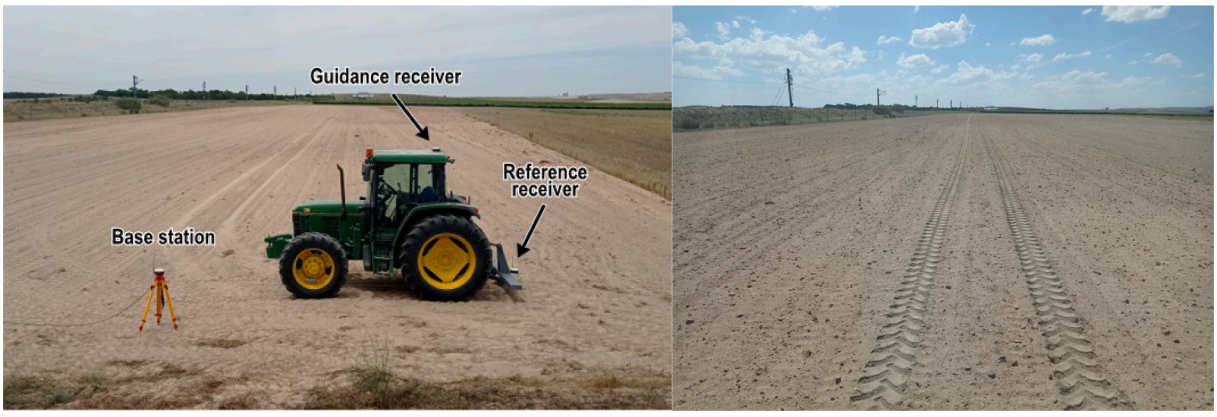


**Fig. 6.** (a) Tractor with the receivers employed in the guidance tests. (b) Straight trajectory followed by the tractor in the guidance tests of configuration C1.

configurations, and, depending on the configuration, was a Navilock NL8022MP, a Novatel Smart2, or a Harxon TS108PRO. This receiver was placed on the tractor cab, on top of the middle of the rear axle, and provided the absolute positioning data for the automatic guidance of the tractor. The second receiver, referred to in this article as the ***reference receiver***, was a Harxon TS108PRO operating with RTK corrections, providing centimetre-level accuracy, mounted on an implement attached to the tractor, and used to capture tractor trajectory for performance analysis. The third receiver, referred to in this article as the ***base station***, was a Harxon TS103, placed on the land where the tests were performed, configured to send RTK messages via the RTCM protocol to the reference receiver via radio during the guidance tests. Fig. 6a shows the guidance receiver, the reference receiver, and the base station.

Two corrections to the positioning data were performed in the guidance tests. The first, roll compensation for the guidance receiver, was performed automatically by the guidance system on the guidance receiver data. Fig. 7a illustrates the geometry associated with this correction, and the graph in Fig. 7b shows the effects of this correction on the guidance receiver trajectory. The second, yaw compensation, was performed in post-processing of the guidance test data, to compute the trajectory of the middle of the rear axle based on the reference receiver trajectory, the yaw angle of the tractor, and the reference trajectory angle. Fig. 7c illustrates the geometry associated with this correction, and Fig. 7d shows the effects on the reference trajectory.

Fourteen guidance tests were performed, one for each configuration. Guidance tests for C1, C2, C3, and C4 were performed on 3 July 2023, guidance tests for C5, C6, C7, C8, C9, and C10 on 4 July 2023, and guidance tests for C11, C12, C13, and C14 on 8 July 2023.

The RMS, mean, and SD errors were computed for guidance tests in short-term intervals and estimated for guidance tests in long-term intervals.

For the short-term, errors were computed in the 300 m trajectory followed by the tractor three times, with the second pass performed 15 minutes after the beginning of the first, and the third pass performed 15 minutes after the beginning of the second. The guidance errors of each configuration were computed based on a relative reference, which was the straight line that closely matched the second trajectory.

For the long-term analysis, fourteen estimations were performed instead of fourteen guidance tests. Each long-term statistical guidance error was considered as the sum of the short-term statistical guidance error and the difference between the long- and short-term statistics of the static test error. This approach is justified because temporal effects are assumed to influence static and guidance tests in the same way.

The mean, being a linear statistic, is estimated using Eq. (1). For RMS and SD, it can be shown mathematically that, assuming the short- and long-term positioning errors are independent of other guidance errors such as control errors, and that these other errors are independent of time and therefore affect short- and long-term measurements equally, RMS and SD can be estimated using Eq. (2) and Eq. (3).

$$\widehat{Mean}\left(G^{long}\right) = Mean\left(G^{short}\right) + Mean\left(P^{long}\right) - Mean\left(P^{short}\right) \quad (1)$$

$$\widehat{RMS}\left(G^{long}\right) = \sqrt{\left(RMS\left(G^{short}\right)\right)^2 + \left(RMS\left(P^{long}\right)\right)^2 - \left(RMS\left(P^{short}\right)\right)^2} \quad (2)$$

$$\widehat{SD}\left(G^{long}\right) = \sqrt{\left(SD\left(G^{short}\right)\right)^2 + \left(SD\left(P^{long}\right)\right)^2 - \left(SD\left(P^{short}\right)\right)^2} \quad (3)$$

### 2.2.6. Colour rules in this document

Authors defined and used four colour rules in this document.

The first colour rule was applied in the short-term static tests, in which the reference was the mean position of the data acquired in the short-term tests (see Fig. 8) Light green colour was used in the presentation of statistics in tables and graphs. This rule was applied to parts a and b of Figs. 9 to 11, to Fig. 15, to Fig. 17, to the first column of Table 1, the first column of Table 3, the first column of Table 4, and to parts a and b of the figures in Appendix B.

The second colour rule was applied in the long-term static tests, in which the reference was the true position of receivers (see Fig. 8). Light red colour was used in the presentation of statistics in tables and graphs in figures. This rule was applied to parts a and b of Figs. 9 to 11, to Fig. 15, to Fig. 17, to the second column of Table 1, the second column of Table 3, the second column of Table 4, and to parts a and b of the figures in Appendix B.

The third colour rule was applied in the short-term guidance tests, in which the reference was the 300 m straight line that closely matched the second trajectory (see Fig. 8). Dark green colour was used in the presentation of statistics in tables and graphs in figures. This rule was applied to Figs. 12 to 16, to the first column of Table 2, the third column of Table 3, the third column of Table 4, and to the figures in Appendix C.

The fourth colour rule was applied in the long-term guidance estimation (see Fig. 8). Dark red colour was used in the presentation of statistics in tables and graphs in figures. This rule was applied to Fig. 15, to Fig. 16, to the second column of Table 2, the fourth column of Table 3, and the fourth column of Table 4.

These four rules are summarised as: (i) green colour is for short-term, (ii) red colour is for long-term, (iii) light colours are for static, and (iv) dark colours are for guidance. Colouring was applied only to the RMS data, because only the RMS statistical error will be used in the final comparison of this article.

### 2.2.7. Methodological considerations

This study takes into account the ISO Standard 12188-2, a standard for testing satellite-based auto-guidance systems. This standard is based on the relative cross-track error (XTE), which is the horizontal distance

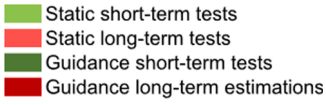


**Fig. 8.** Colours employed to present statistics in tables and graphs in figures. Green is used for short-term tests and red for long-term tests. Light colours are for static tests and dark colours for guidance tests.

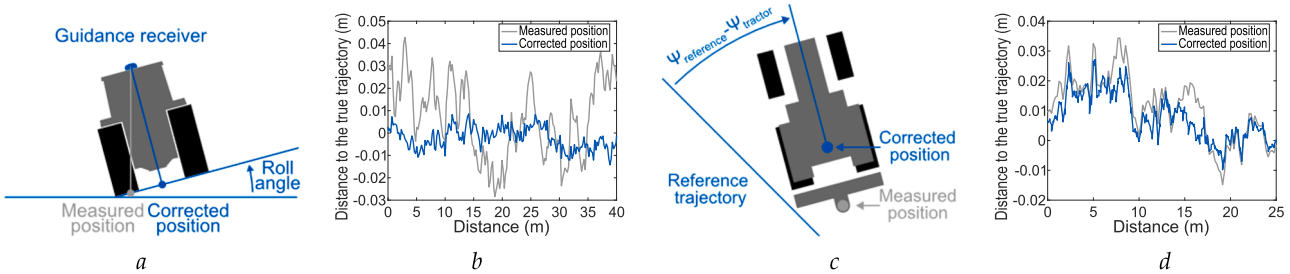


**Fig. 7.** Corrections made in the guidance tests. (a) Illustration of the roll compensation geometry. (b) Real example in our tests of the roll compensation. (c) Illustration of the yaw compensation. (d) Real example in our tests of the yaw compensation.

between any given position of the tractor and the track that the tractor tries to follow, which was recorded during any previous test run over the same test course. Based on the XTE, this standard presents two measurements of performance: the pass-to-pass guidance error and the long-term guidance error. This standard defines pass-to-pass guidance error as the XTE with a revisit time below 15 minutes, which is equivalent to the short-term error of our article, and also defines the long-term guidance error as the XTE with a revisit time above 1 hour. This study also takes into account the guidelines of Rounsaville et al. to compute the XTE following the recommendation of the ISO Standard 12188-2 (Rounsaville et al., 2016).

## 3. Results

### 3.1. Results of static tests

#### 3.1.1. Graphical positioning error analysis with scatter plots, cumulative distribution functions, and 15-minute positioning error evolution

Fig. 9a, Fig. 10a, and Fig. 11a show the scatter plots of the acquired positions in NED Cartesian coordinates during the 24-hour static tests for configurations C1, C5 and C14. Light blue points represent the first 8 hours, blue points the 9$^{th}$–16$^{th}$ hours, and dark blue points the 17$^{th}$–24$^{th}$ hour. To present a viewable number of points, only one every 100 points

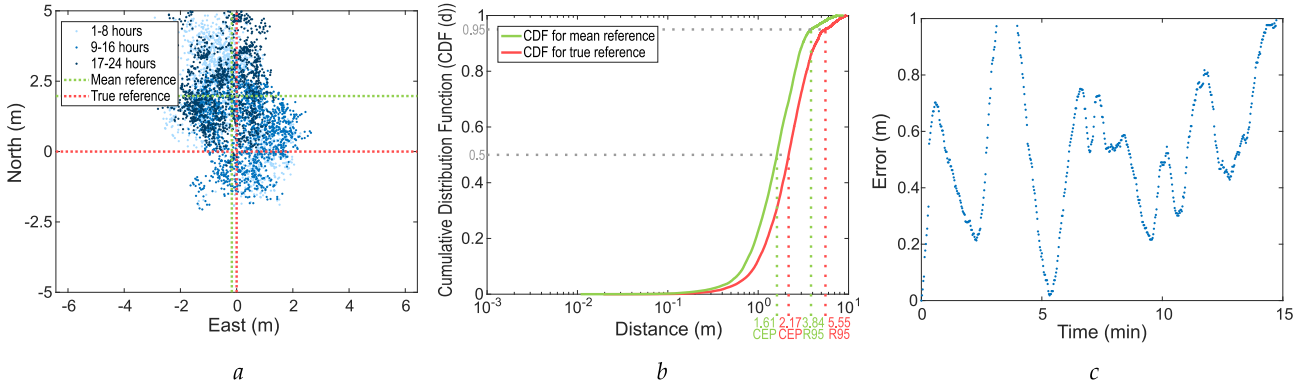


**Fig. 9.** C1 (Navilock). Graphs obtained in the static test of the Navilock NL8022MP receiver with EGNOS off: (a) Scatter plot for 24 hours, in which 5.42% of the points are outside the limits of this plot; (b) Cumulative Distribution Function of the distances of measured positions to the mean and true reference positions from the 24-hour static tests; and (c) Evolution of the distance error with respect to the initial point, in which some points before 26 minutes, and all points after 26 minutes, are higher than 1 m, and are outside this graph.

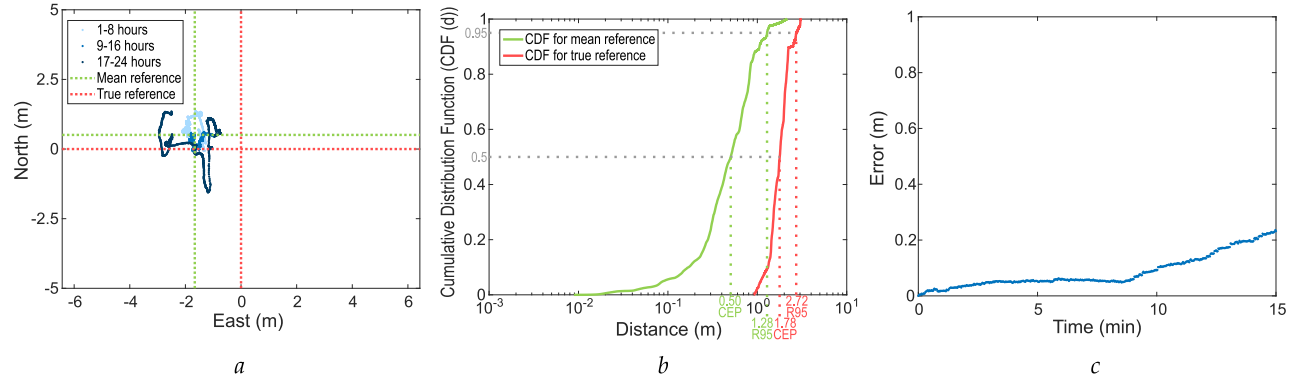


**Fig. 10.** C5 (Novatel|EGNOS|GLIDE). Graphs obtained in the static test of the Novatel Smart2 receiver with EGNOS on and GLIDE on: (a) Scatter plot for 24 hours; (b) Cumulative Distribution Function of the distances of measured positions to the mean and true reference positions from the 24-hour static tests; and (c) Evolution of the distance error with respect to the initial point.

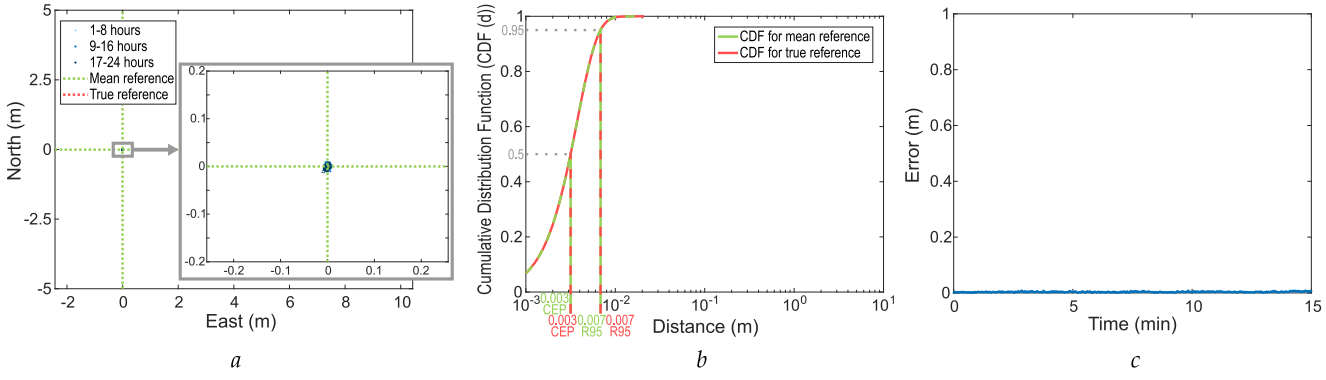


**Fig. 11.** C14 (Harxon|On-site RTK). Graphs obtained in the static test of the Harxon TS108PRO receiver with RTK via base station located some metres from the receiver: (a) Scatter plot for 24 hours; (b) Cumulative Distribution Function of the distances of measured positions to the mean and true reference positions from the 24-hour static tests; and (c) Evolution of the distance error with respect to the initial point.

**Table 1**
RMS, Mean, SD, CEP, R95 and R99.7 errors computed in the static tests. Augmentation types that each receiver achieved in its static tests, expressed in percentage of time.

| Configurations | Static positioning error (m) | | | | | | | | | | | | Augmentation type (% time) |
|---|---|---|---|---|---|---|---|---|---|---|---|---|---|
| | RMS error | | Mean error | | SD | | CEP error | | R95 error | | R99.7 error | | |
| | short-term | long-term | short-term | long-term | short-term | long-term | short-term | long-term | short-term | long-term | short-term | long-term | |
| C1 (Navilock) | 0.647 | 2.933 | 0.578 | 2.489 | 0.288 | 1.552 | 0.546 | 2.173 | 1.113 | 5.554 | 1.295 | 9.059 | none |
| C2 (Navilock\|EGNOS) | 1.022 | 2.136 | 0.908 | 1.876 | 0.468 | 1.022 | 0.851 | 1.735 | 1.777 | 3.725 | 2.108 | 5.601 | 100% EGNOS |
| C3 (Novatel) | 0.546 | 2.331 | 0.480 | 2.073 | 0.249 | 1.065 | 0.436 | 1.988 | 0.964 | 3.971 | 1.149 | 6.874 | none |
| C4 (Novatel\|EGNOS) | 0.386 | 1.442 | 0.345 | 1.364 | 0.170 | 0.469 | 0.331 | 1.347 | 0.658 | 2.117 | 0.771 | 3.121 | 100% EGNOS |
| C5 (Novatel\|EGNOS\|GLIDE) | 0.061 | 1.867 | 0.054 | 1.811 | 0.028 | 0.453 | 0.054 | 1.778 | 0.104 | 2.724 | 0.117 | 3.042 | 100% EGNOS |
| C6 (Harxon) | 0.195 | 1.466 | 0.168 | 1.292 | 0.093 | 0.694 | 0.152 | 1.132 | 0.355 | 2.878 | 0.423 | 3.548 | none |
| C7 (Harxon\|EGNOS) | 0.164 | 1.094 | 0.143 | 1.051 | 0.079 | 0.303 | 0.131 | 1.064 | 0.295 | 1.513 | 0.359 | 1.987 | 100% EGNOS |
| C8 (Harxon\|RTK\|645km) | 0.303 | 0.733 | 0.273 | 0.659 | 0.131 | 0.321 | 0.260 | 0.646 | 0.506 | 1.183 | 0.600 | 1.592 | 100% DGNSS |
| C9 (Harxon\|RTK\|296km) | 0.057 | 0.238 | 0.059 | 0.198 | 0.025 | 0.133 | 0.048 | 0.173 | 0.099 | 0.429 | 0.119 | 1.111 | 95.5% float RTK, 4.5% DGNSS |
| C10 (Harxon\|RTK\|100km) | 0.014 | 0.094 | 0.012 | 0.061 | 0.006 | 0.071 | 0.011 | 0.025 | 0.023 | 0.215 | 0.028 | 0.241 | 100% fixed RTK |
| C11 (Harxon\|RTK\|42km) | 0.008 | 0.016 | 0.007 | 0.014 | 0.004 | 0.009 | 0.007 | 0.012 | 0.014 | 0.031 | 0.017 | 0.044 | 100% fixed RTK |
| C12 (Harxon\|RTK\|14km) | 0.006 | 0.012 | 0.006 | 0.011 | 0.003 | 0.006 | 0.005 | 0.010 | 0.011 | 0.022 | 0.014 | 0.031 | 100% fixed RTK |
| C13 (Harxon\|VRS-NRTK\|14,25,42km) | 0.007 | 0.011 | 0.006 | 0.009 | 0.003 | 0.006 | 0.005 | 0.008 | 0.012 | 0.021 | 0.017 | 0.041 | 100% fixed RTK |
| C14 (Harxon\|On-site RTK) | 0.003 | 0.004 | 0.002 | 0.003 | 0.001 | 0.002 | 0.002 | 0.003 | 0.005 | 0.007 | 0.007 | 0.010 | 100% fixed RTK |

is plotted. The scatter plot in Fig. 11a is highly concentrated, so a zoomed view is included for better visualization.

Fig. 9b, Fig. 10b, and Fig. 11b present the cumulative distribution functions (CDFs) of distances from measured positions to the mean and true reference positions for the same configurations. CEP and R95 values are marked with horizontal and vertical dotted lines. A logarithmic x-axis allows comparison of low- and high-precision configurations on the same scale.

Fig. 9c, Fig. 10c, and Fig. 11c show the evolution of distance errors relative to the initial point during the first 15 minutes for the same configurations. Distances were computed from the first point acquired in each configuration. To improve visual clarity, only one in every eight points is shown.

Fig. 9, Fig. 10, and Fig. 11 show the static test results for three representative configurations: low-cost C1 without augmentation, mid-range C5 with GLIDE, and high-end C14 with on-site RTK. Appendix B presents the graphs of the 14 configurations (Fig. B.1 to Fig. B.14).

Fig. B.1a to Fig. B.14a illustrate two key aspects: (i) The plots show a decreasing trend in size from C1 to C14; the final configurations are compact, requiring a zoomed view from Fig. B.10. RTK with baselines shorter than 100 km yields errors of only a few centimetres, showing larger errors in early configurations. (ii) The mean reference is centred in all configurations; the real reference is centred from C9 onwards, so from C9 performance relative to the mean approximates performance relative to the real reference.

Fig. B.1b to Fig. B.14b illustrate two key aspects: (i) The first configurations show an S-shaped curve on the right, whereas the last on the left, indicating larger errors in early configurations. (ii) The first configurations show differences between CDFs for mean and true references, while the last configurations are similar, indicating comparable performance.

Fig. B.1c to Fig. B.14c illustrate three key aspects: (i) C1–C4 and C6–C9 show rapid error increase, indicating poor short-term performance; long-term errors are likely higher. These correspond to unaugmented, EGNOS, and RTK with long baselines. (ii) C5 shows slow, steady error growth, indicating good short-term but limited long-term performance; this corresponds to GLIDE. (iii) C11–C14 exhibit very low, nearly flat errors, indicating good short- and long-term performance; these correspond to RTK with medium/short baselines, VRS-NRTK with short baselines, and on-site RTK.

#### 3.1.2. Numerical positioning error analysis with RMS, mean, SD, CEP, R95 and R99.7 error statistics and percentage of augmentation types

The RMS error, the mean error, the mean distance to the reference point, the SD, the CEP error, the R95 error, and the R99.7 error of static tests, computed as described in the Variables under study section, are presented in Table 1. This table also presents the augmentation type that each receiver achieved in its static test, expressed as the percentage of time for each type, because the receiver of configuration C9 changed the augmentation type during the test. The information on the augmentation type was obtained from the GGA NMEA sentence, as described in Appendix A.2.

Table 1 confirms the key aspects illustrated graphically in Fig. B.1 to Fig. B.14. Additionally, it reveals the following insights: (i) Unaugmented positioning achieves decimetre-level precision in the short term and metre-level accuracy in the long term for configurations C1, C3, and C6; (ii) EGNOS slightly improves unaugmented positioning in all cases, except in the short term for configuration C2; (iii) GLIDE yields good short-term performance but poor long-term results for configuration C5; (iv) RTK and NRTK provide centimetre-level positioning for short baseline lengths for configurations C11 to C14; (v) RTK error tends to increase with baseline length for configurations C8 to C14; (vi) long-term error is consistently greater than short-term error across all configurations; (vii) A fixed RTK solution is achievable with baseline lengths under 100 km for configurations C10 to C14.

### 3.2. Results of guidance tests

#### 3.2.1. Graphical guidance error analysis along a trajectory of 300 m

Fig. 12, Fig. 13, and Fig. 14 show, for configurations C1, C5, and C14, the trajectories followed by the tractor. Each figure shows the error in three evaluations of the guidance along a horizontal straight trajectory of 300 m, using a thin green line for the first evaluation, a medium green line for the second evaluation performed 15 minutes after the first evaluation, and a thick green line for the third evaluation performed 30 minutes after the first evaluation. The relative reference represents the 300 m straight line that closely matched the second trajectory. To graphically compare the guidance with a wide precision range, each figure has three graphs: the first scaled to represent vertical errors between -5 and 5 metres, the second scaled to represent vertical errors between -50 and 50 cm, and the third scaled to represent vertical errors between -10 and 10 cm.

Fig. 12, Fig. 13, and Fig. 14 show the guidance test graphical results of a representative subset of three out of the 14 configurations tested: the low-cost C1 configuration without augmentation, the mid-range C5 configuration with GLIDE, and the high-end C14 configuration with on-site RTK. Appendix C presents the graphs of the 14 configurations tested in this study from Fig. C.1 to Fig. C.14.

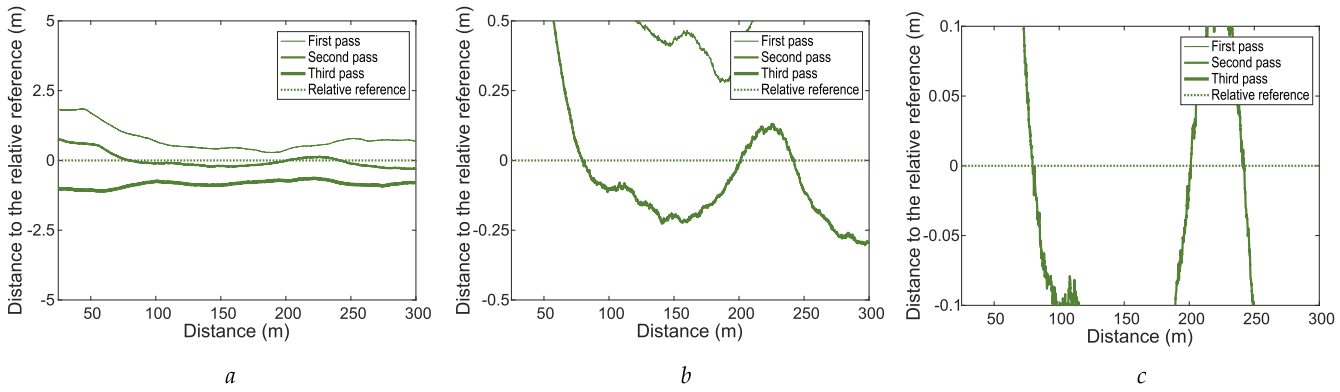


**Fig. 12.** C1 (Navilock). Graphs showing the guidance test short-term error of the Navilock NL8022MP receiver with EGNOS off, with the ordinate axis ranging from: (a) -5 to 5 m, (b) -0.5 to 0.5 m, (c) -0.1 to 0.1 m.

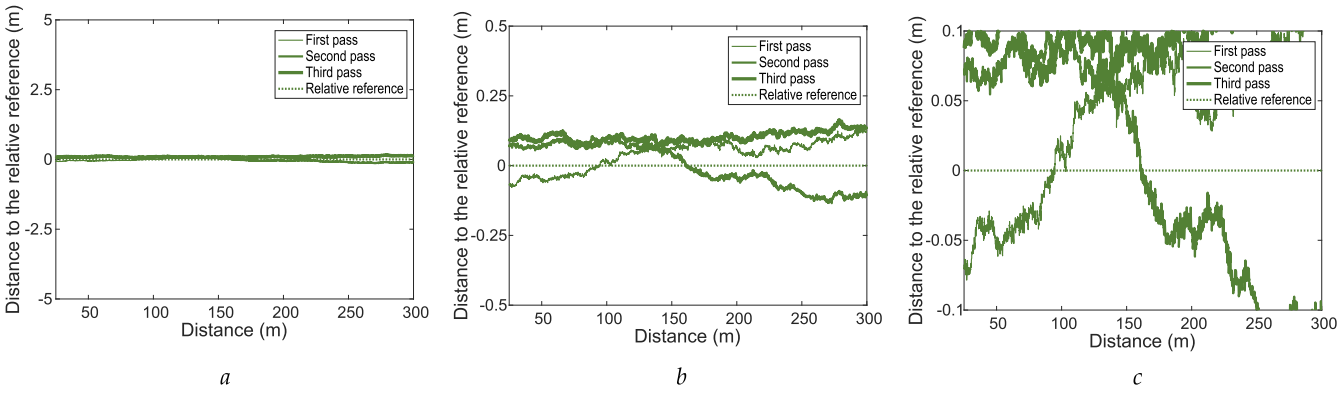


**Fig. 13.** C5 (Novatel|EGNOS|GLIDE). Graphs showing the guidance test short-term error of the Novatel Smart2 receiver with EGNOS on and GLIDE on, with the ordinate axis ranging from: (a) -5 to 5 m, (b) -0.5 to 0.5 m, (c) -0.1 to 0.1 m.

The guidance graphs from Fig. C.1 to Fig. C.14 illustrate several key aspects. Specifically: (i) The first, second, and third passes, performed 15 minutes apart, are displaced relative to one another, particularly in the unaugmented configurations or those augmented only with EGNOS, as shown in Fig. C.1 to Fig. C.4 and Fig. C.6 to Fig. C.7, indicating that these configurations produce a significant guidance error that is expected to increase over the long term; (ii) EGNOS slightly improves guidance by the Novatel and Harxon receivers with respect to unaugmented configurations, as shown in Fig. C.3, Fig. C.4, Fig. C.6 and Fig. C.7, but slightly worsens the guidance with the Navilock receiver, as shown in Fig. C.1 and Fig. C.2 (iii) GLIDE notably improves the guidance in the three spaced passes at 15-minute intervals, as shown in Fig. C.4 and Fig. C.5; and (iv) RTK and NRTK provide centimetre-level guidance for short baseline lengths, as shown in Fig. C.11 to Fig. C.14.

### *3.2.2. Numerical guidance error analysis with RMS, mean and SD error statistics and percentages of augmentation types*

Table 2 presents three statistical parameters computed from the data of the guidance test for each configuration: (i) the RMS error, (ii) the mean error, and (iii) the SD. In this column, the short-term data are statistics of guidance tests measurements, and the long-term data are estimations, being statistics and estimations computed as described in the Methodology of guidance tests section. This table also presents the augmentation type that each receiver achieved during its guidance test, expressed as the percentage of time with each type, because some receivers changed the augmentation type during the test.

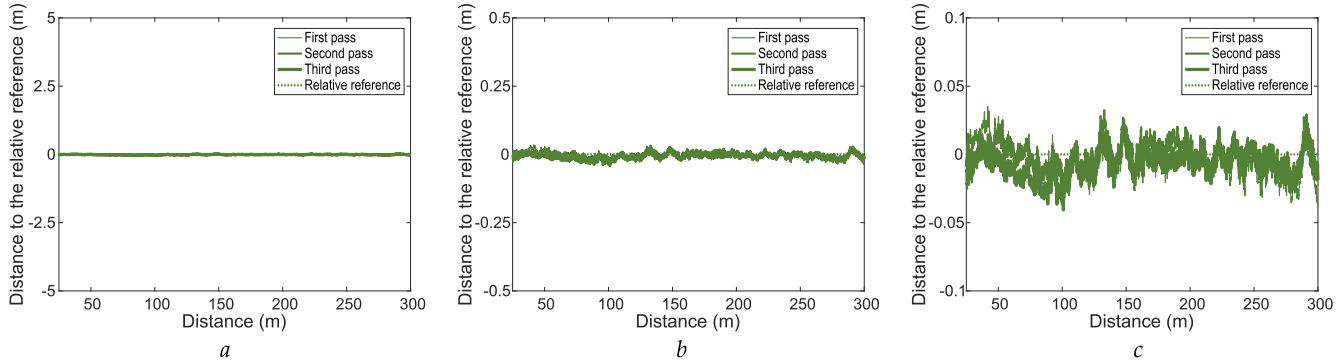


**Fig. 14.** C14 (Harxon|On-site RTK). Graphs showing the guidance test short-term error of the Harxon TS108PRO receiver with RTK via a base station located a few metres from the receiver, with the ordinate axis ranging from: (a) -5 to 5 m, (b) -0.5 to 0.5 m, (c) -0.1 to 0.1 m.

**Table 2**
RMS, mean error, SD, and percentage of time each augmentation type was achieved by the receivers in guidance tests. The long-term data are estimates rather than direct statistics from measurements, computed as described in the Methodology of guidance tests section.

| Configurations | Guidance error (m) | | | | | | Augmentation type (% time) |
|---|---|---|---|---|---|---|---|
| | RMS error | | Mean error | | SD | | |
| | short-term (measured) | long-term (estimated) | short-term (measured) | long-term (estimated) | short-term (measured) | long-term (estimated) | |
| C1 (Navilock) | 0.865 | 2.989 | 0.804 | 2.715 | 0.319 | 1.558 | none |
| C2 (Navilock\|EGNOS) | 1.905 | 2.673 | 1.871 | 2.839 | 0.361 | 0.978 | 100% EGNOS |
| C3 (Novatel) | 0.793 | 2.401 | 0.780 | 2.373 | 0.145 | 1.046 | none |
| C4 (Novatel\|EGNOS) | 0.470 | 1.467 | 0.432 | 1.451 | 0.183 | 0.474 | 100% EGNOS |
| C5 (Novatel\|EGNOS\|GLIDE) | 0.087 | 1.868 | 0.081 | 1.838 | 0.032 | 0.453 | 100% EGNOS |
| C6 (Harxon) | 0.515 | 1.542 | 0.505 | 1.629 | 0.098 | 0.695 | none |
| C7 (Harxon\|EGNOS) | 0.444 | 1.169 | 0.397 | 1.305 | 0.199 | 0.354 | 100% EGNOS |
| C8 (Harxon\|RTK\|645km) | 0.502 | 0.835 | 0.418 | 0.804 | 0.279 | 0.405 | 100% DGNSS |
| C9 (Harxon\|RTK\|296km) | 0.239 | 0.332 | 0.221 | 0.368 | 0.092 | 0.160 | 33% float RTK, 67% DGNSS |
| C10 (Harxon\|RTK\|100km) | 0.173 | 0.196 | 0.120 | 0.169 | 0.124 | 0.143 | 33% fixed RTK, 67% float RTK |
| C11 (Harxon\|RTK\|42km) | 0.028 | 0.031 | 0.023 | 0.030 | 0.017 | 0.019 | 90.5% fixed RTK, 9.5% float RTK |
| C12 (Harxon\|RTK\|14km) | 0.023 | 0.025 | 0.019 | 0.024 | 0.013 | 0.014 | 100% fixed RTK |
| C13 (Harxon\|VRS-NRTK\|14,25,42km) | 0.014 | 0.016 | 0.010 | 0.013 | 0.009 | 0.010 | 100% fixed RTK |
| C14 (Harxon\|On-site RTK) | 0.012 | 0.013 | 0.010 | 0.011 | 0.008 | 0.008 | 100% fixed RTK |

Table 2 confirms the key aspects identified in static test results (*Section 3.1*) and in the guidance test graphs (Appendix C and *Section 3.2.1*). Specifically: (i) unaugmented guidance achieves decimetre-level precision in the short term and metre-level accuracy in the long term, as seen in configurations C1, C3, and C6 in Table 2; (ii) EGNOS slightly improves unaugmented guidance in all cases, except in the short term for configuration C2, as seen in configurations C2, C4, and C7; (iii) GLIDE yields good short-term performance in guidance but poor long-term performance, as seen in configuration C5; (iv) RTK and NRTK provide centimetre-level guidance for short baseline lengths, as seen in configurations C11 to C14; (v) RTK guidance error tends to increase with baseline length, as evidenced in configurations C8 to C14; (vi) long-term guidance error is consistently greater than short-term error across all configurations; and (vii) a fixed RTK solution is achievable with baseline lengths under 100 km, as evidenced by configurations C10 to C14.

### 3.3. Results comparison

A comparison of positioning and guidance for both, short- and long-term, is presented in Table 3, in which four columns summarise the performance of the 14 configurations tested. Concretely:

The first column presents the short-term RMS positioning errors in the static tests. The values of this column come from Column 1 of Table 1. The errors in this column are exclusively positioning errors of receivers.

The second column presents the long-term RMS positioning errors of each configuration in the static tests. The values of this column come from Column 2 of Table 1. The errors in this column are exclusively positioning errors of receivers.

The third column presents the short-term RMS errors computed in the guidance tests. The values of this column come from Column 1 of Table 2. The errors in this column are the total errors in the guidance, composed of the positioning errors of guidance receivers, plus the guidance errors that the guidance system makes trying to follow the desired trajectory.

The fourth column presents an estimation of the long-term RMS errors for the 14 receivers used to guide the tractor. This estimation is performed according to Eq. (2) presented in the Methodology of guidance tests section.

Confidence intervals of the RMS errors were computed for short-term and long-term static tests, as well as for short-term guidance tests. For example, for the C1 static test error reported in Table 3, the estimated RMS error value was 0.640. The associated 95% confidence interval was very narrow, with absolute margins of approximately $\pm 8.6 \cdot 10^{-4}$ around

**Table 3**
RMS errors computed for the 14 configurations in the static tests for both short- and long-term, and in the guidance tests for both short- and long-term.

| Positioning device | Static tests | | Guidance tests | |
|---|---|---|---|---|
| | Short-term positioning RMS error (m) measured | Long-term positioning RMS error (m) measured | Short-term guidance RMS error (m) measured | Long-term guidance RMS error (m) estimated |
| C1 (Navilock) | 0.647 | 2.933 | 0.865 | 2.989 |
| C2 (Navilock\|EGNOS) | 1.022 | 2.136 | 1.905 | 2.673 |
| C3 (Novatel) | 0.546 | 2.331 | 0.793 | 2.401 |
| C4 (Novatel\|EGNOS) | 0.386 | 1.442 | 0.470 | 1.467 |
| C5 (Novatel\|EGNOS\|GLIDE) | 0.061 | 1.867 | 0.087 | 1.868 |
| C6 (Harxon) | 0.195 | 1.466 | 0.515 | 1.542 |
| C7 (Harxon\|EGNOS) | 0.164 | 1.094 | 0.444 | 1.169 |
| C8 (Harxon\|RTK\|645km) | 0.303 | 0.733 | 0.502 | 0.835 |
| C9 (Harxon\|RTK\|296km) | 0.057 | 0.238 | 0.239 | 0.332 |
| C10 (Harxon\|RTK\|100km) | 0.014 | 0.094 | 0.173 | 0.196 |
| C11 (Harxon\|RTK\|42km) | 0.008 | 0.016 | 0.028 | 0.031 |
| C12 (Harxon\|RTK\|14km) | 0.006 | 0.012 | 0.023 | 0.025 |
| C13 (Harxon\|VRS-NRTK\|14,25,42km) | 0.007 | 0.011 | 0.014 | 0.016 |
| C14 (Harxon\|On-site RTK) | 0.003 | 0.004 | 0.012 | 0.013 |

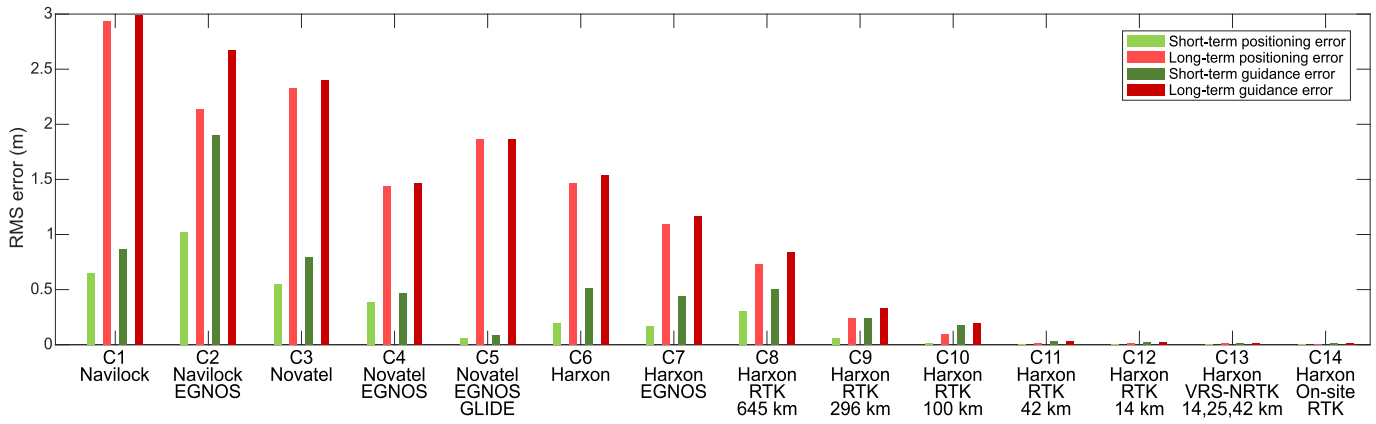


**Fig. 15.** RMS errors computed for the 14 configurations in the static tests for both short- and long-term, and in the guidance tests for short- and long-term. The ordinate axis is presented on a linear scale, to allow visual comparison of the RMS errors across the 14 configurations.

the central estimate, corresponding to relative margins of approximately ±0.14%. This value, as well as all other values in the table, showed relative errors below 1%. The narrow confidence intervals indicate a high precision of the RMS estimates, suggesting a limited influence of random fluctuations or localised variations on the results. No confidence intervals were computed for long-term guidance RMS errors, as these values were derived from estimations rather than from direct measurements.

The data of Table 3 are presented in Fig. 15. The errors of C11 to C14 configurations in this figure are tiny compared with those of C1 to C10 configurations.

Table 4 summarizes the short- and long-term performance results for the augmentation systems assessed in this study: unaugmented, EGNOS, GLIDE, RTK at different baseline lengths, VRS-NRTK, and on-site RTK: (i) the unaugmented values correspond to the mean of RMS errors obtained with the Navilock, Novatel and Harxon receivers from configurations C1, C3, and C6; (ii) the EGNOS values correspond to the mean of RMS errors obtained with the Novatel and Harxon receivers from configurations C4 and C7, having excluded the data obtained with the Navilock receiver in configuration C2 due to inconsistency, as EGNOS did not improve in this receiver and even worsened it; (iii) the GLIDE values correspond to the errors obtained with the Novatel receiver from configuration C5; (iv) the long baseline RTK values correspond to the mean of RMS errors obtained with the Harxon receiver from

**Table 4**
RMS error obtained in short- and long-term tests for the principal positioning modes assessed in this study: unaugmented, EGNOS, GLIDE, RTK for different baseline lengths, VRS-NRTK and on-site RTK. Each error value is the mean of the RMS error values obtained in the configurations that use each positioning mode.

| | Short-term positioning RMS error (m) measured | Long-term positioning RMS error (m) estimated | Short-term guidance RMS error (m) measured | Long-term guidance RMS error (m) estimated |
|---|---|---|---|---|
| Unaugmented (C1, C3 and C6) | 0.463 | 2.243 | 0.724 | 2.310 |
| EGNOS (C4 and C7) | 0.275 | 1.268 | 0.457 | 1.318 |
| GLIDE (C5) | 0.061 | 1.867 | 0.087 | 1.868 |
| Long baseline RTK (C8, C9 and C10) | 0.125 | 0.355 | 0.305 | 0.455 |
| Medium baseline RTK (C10 and C11) | 0.011 | 0.055 | 0.101 | 0.114 |
| Short baseline RTK (C12) | 0.006 | 0.012 | 0.023 | 0.025 |
| VRS-NRTK (C13) | 0.007 | 0.011 | 0.014 | 0.016 |
| On-site RTK (C14) | 0.003 | 0.004 | 0.012 | 0.013 |

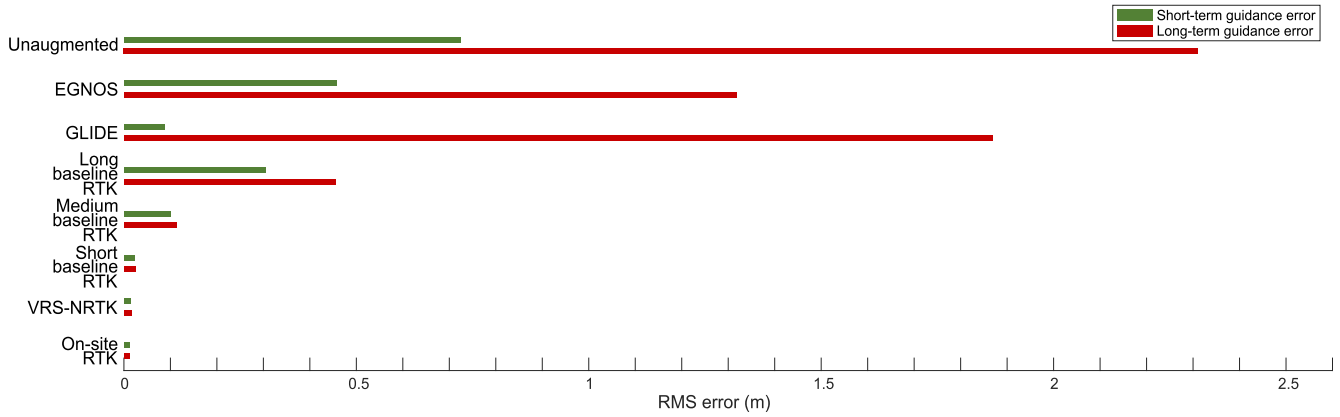


**Fig. 16.** Representation of RMS errors obtained in short- and long-term guidance tests for the principal positioning modes assessed in this study: unaugmented, EGNOS, GLIDE, RTK for different baseline lengths, VRS-NRTK and on-site RTK.

configurations C8, C9, and C10, receiving RTK augmentation from base stations located 645, 296, and 100 km away from the tractor; (v) the medium baseline RTK values correspond to the mean of RMS errors obtained with the Harxon receiver from configurations C10 and C11, receiving RTK augmentation from base stations located 100 and 42 km away; (vi) the short baseline RTK values correspond to the mean of RMS errors obtained with the Harxon receiver from configurations C12 and C13: in C12, RTK augmentation was provided by a base station located 14 km away, whereas in C13, augmentation was provided via the VRS technique using several base stations located at distances of 14 km or more; and (vii) the on-site RTK values correspond to the errors obtained with the Harxon receiver from configuration C14. Fig. 16 shows the values of this table for guidance tests.

The next subsections summarise the results obtained for each analysed augmentation system.

### 3.3.1. Unaugmented

Unaugmented GNSS (C1, C3, and C6) results are summarised as follows:

- Unaugmented RMS errors, based on averaged results from the Navilock, Novatel, and Harxon receivers, were 0.463 m in short-term static tests, 0.724 m in short-term guidance, 2.243 m in long-term static, and 2.310 m in long-term guidance (Table 4). Therefore, unaugmented positioning yielded short-term static and guidance RMS errors below 1 m, and long-term static and guidance RMS errors in the 2–3 m range.
- The Novatel receiver outperformed the Navilock receiver under unaugmented conditions. RMS errors for the unaugmented Navilock (C1) were 0.647 m in short-term static tests, 0.865 m in short-term guidance, 2.933 m in long-term static, and 2.989 m in long-term guidance (Table 3). Corresponding errors for the Novatel (C3) were 0.546 m, 0.793 m, 2.331 m, and 2.401 m, resulting in improvements of approximately 0.101 m (16%), 0.072 m (8%), 0.602 m (21%), and 0.588 m (20%), respectively (Table 3). Therefore, the mean improvement of the mid-range Novatel over the low-cost Navilock was approximately 16%.
- The Harxon receiver outperformed the Navilock receiver under unaugmented conditions. RMS errors for the unaugmented Navilock (C1) were 0.647 m in short-term static tests, 0.865 m in short-term guidance, 2.933 m in long-term static, and 2.989 m in long-term guidance (Table 3). Corresponding errors for the Harxon (C6) were 0.195 m, 0.515 m, 1.466 m, and 1.542 m, resulting in improvements of approximately 0.452 m (70%), 0.350 m (40%), 1.467 m (50%), and 1.447 m (48%), respectively (Table 3). Therefore, the mean improvement of the high-end Harxon over the low-cost Navilock was approximately 52%.

### 3.3.2. EGNOS

EGNOS (C4 and C7) RMS errors, based on averaged results from the Novatel and Harxon receivers, were 0.275 m and 0.457 m for short-term static and guidance, while long-term errors increased to 1.268 m and 1.318 m (Table 4). The corresponding errors for unaugmented GNSS were 0.463 m, 0.724 m, 2.243 m, and 2.310 m, resulting in improvements of approximately 0.188 m (41%), 0.267 m (37%), 0.975 m (43%), and 0.992 m (43%), respectively. Therefore, EGNOS showed (i) short-term static and guidance RMS errors below 60 cm, (ii) long-term static and guidance RMS errors in the 1–2 m range, and (iii) a mean RMS error reduction of approximately 41% compared to unaugmented GNSS.

### 3.3.3. GLIDE

GLIDE (C5) RMS errors were 6.1 and 8.7 cm for short-term static and guidance tests, while long-term errors increased to 1.867 m and 1.868 m (Table 4). Therefore, GLIDE yielded errors below 20 cm in the short term, with no improvement over EGNOS in the long term.

### 3.3.4. RTK

RTK (C8–C12) results are summarised as follows:

- The accuracy of the Harxon TS108PRO operating in RTK mode, according to manufacturer specifications, is 10 mm + 1 ppm as a function of the baseline length. This means that the RMS error should equal 10 mm plus 1 mm for each kilometre of baseline length. In our study, configurations C8, C9, C10, C11, C12, and C14 used baselines of 645, 296, 100, 42, 14, and 0 km, yielding short-term static errors of 0.303, 0.057, 0.014, 0.008, 0.006, and 0.003 m, and long-term static errors of 0.733, 0.238, 0.094, 0.016, 0.012, and 0.004 m, as shown in Table 3. Fig. 17 plots these short-term errors as light green circles and the long-term errors against baseline length, with the Harxon specification represented by a blue line.

  As shown in Fig. 17, the close alignment between the red circles and the blue line confirms that long-term errors follow the baseline-length dependence stated in the specifications, whereas the green circles lying well below the blue line indicate a weaker short-term dependence than specified.
- Long-baseline RTK results, using single-base stations at 645 km (C8), 296 km (C9), and 100 km (C10), showed: short-term static RMS errors of 30.3, 5.7, and 1.4 cm; long-term static RMS errors of 73.3, 23.8, and 9.4 cm; short-term guidance RMS errors of 50.2, 23.9, and 17.3 cm; and long-term guidance RMS errors of 83.5, 33.2, and 19.6 cm (Table 3). Therefore, the Harxon TS108PRO, operating in RTK mode with baselines exceeding 100 km, yielded positioning RMS errors in the 1.4–73.3 cm range and guidance RMS errors in the 17.3–83.5 cm range.
- Medium-baseline RTK results, using single-base stations at 100 km (C10) and 42 km (C11), showed: short-term static RMS errors of 1.4 and 0.8 cm; long-term static RMS errors of 9.4 and 1.6 cm; short-term guidance RMS errors of 17.3 and 2.8 cm; and long-term guidance RMS errors of 19.6 and 3.1 cm (Table 3). Therefore, the Harxon TS108PRO, operating in RTK mode with baselines between 20 and 100 km, yielded positioning RMS errors in the 0.8–9.4 cm range and guidance RMS errors in the 2.8–19.6 cm range.
- Short-baseline RTK errors using a single-base station located at 14 km (C12) were 0.6 cm in short-term static tests, 2.3 cm in short-term guidance, 1.2 cm in long-term static, and 2.5 cm in long-term guidance (Table 3). Therefore, the Harxon TS108PRO, operating in RTK mode with a baseline shorter than 20 km, yielded positioning RMS

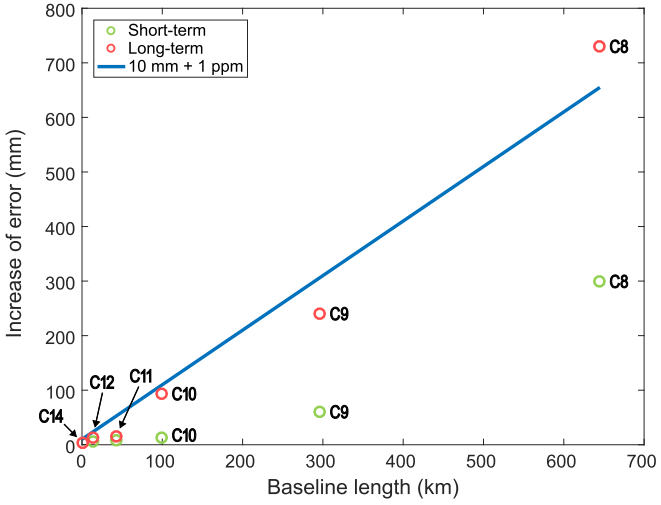


**Fig. 17.** Error of the Harxon TS108PRO as a function of baseline length (i) according to its datasheet (blue line), (ii) measured in static short-term tests (light green circles), and (iii) measured in static long-term tests (light red circles).

errors in the 0.6–1.2 cm range, and guidance RMS errors in the 2.3–2.5 cm range.

- Position solutions in RTK mode (C8–C14) can be fixed, float, or DGNSS. As shown in Table 1 and Table 2, the 645 km baseline (C8) was consistently in DGNSS, the 296 km baseline (C9) alternated between DGNSS and float RTK, the 100 km and 42 km baselines (C10, C11) alternated between float and fixed RTK, and the 14 km and 0 km baselines (C12–C14) were consistently in fixed RTK. Therefore, our study reported float or DGNSS solutions with long baselines exceeding 100 km, fixed or float solutions with medium baselines between 20 and 100 km, and fixed solutions with short baselines of less than 20 km.

#### 3.3.5. VRS-NRTK

VRS-NRTK (C13) RMS errors, with the three nearest base stations at 14, 25, and 42 km, were 0.7 cm in short-term static tests, 1.4 cm in short-term guidance, 1.1 cm in long-term static, and 1.6 cm in long-term guidance (Table 4). For C12 in single-base mode with a 14 km baseline, the corresponding errors were 0.6, 2.3, 1.2, and 2.5 cm, respectively (Table 4). These correspond to improvements of approximately −0.1 cm (−17%), 0.9 cm (39%), 0.1 cm (8%), and 0.9 cm (36%), indicating that the use of the VRS technique yields a mean improvement of about 17% over single-base short-baseline RTK, with guidance RMS errors in the 1.4–1.6 cm range.

#### 3.3.6. On-site RTK

On-site RTK (C14) RMS errors were 0.3 cm in short-term static tests, 1.2 cm in short-term guidance, 0.4 cm in long-term static, and 1.3 cm in long-term guidance (Table 4). Therefore, on-site RTK yielded positioning RMS errors in the 0.3–0.4 cm range, and guidance RMS errors in the 1.2–1.3 cm range.

## 4. Discussion

### 4.1. Findings

Several findings emerge from the results obtained with unaugmented GNSS and using EGNOS, GLIDE, RTK, VRS-NRTK, and on-site RTK augmentation systems.

#### 4.1.1. Unaugmented

Unaugmented results from this study showed: (i) short-term static and guidance RMS errors below 1 m, (ii) long-term static and guidance RMS errors in the 2–3 m range, (iii) improvements of 16% when using the Novatel mid-range receiver compared to the Navilock low-cost receiver, and (iv) improvements of 52% when using the Harxon high-end receiver compared to the Navilock low-cost receiver (*Section 3.3.1*). These errors obtained in our tests are consistent with those reported by government agencies for major GNSS constellations, with R95 positioning errors ranging from below 5 m for Galileo and GLONASS to around 9 m for GPS and BeiDou (China Satellite Navigation Office, 2021; EUSPA, 2024; Renfro et al., 2020; Russian Defence Ministry and Roscosmos State Corporation, 2020). The unaugmented positioning errors obtained in our tests are also consistent with previous studies that reported mean errors of 0.9–14.4 m (Sun et al., 2017) and ≤ 9 m (Shi et al., 2020); RMS errors of 0.8–5.4 m (Zhang and Pan, 2022), 3–5 m (Kaplan and Hegarty, 2017), and 0.32–5.94 m (Karimi, 2021); and CEP errors of 1–5 m (Mahato et al., 2024a, 2024c). No studies on guidance of tractors or other vehicles with unaugmented positioning were found. Overall, our results, reports from government agencies, and results from other researchers indicate that unaugmented positioning typically results in short-term guidance RMS errors below 1 m, which increase to 2–3 m in the long term, with variations of around 50% depending on receiver quality.

#### 4.1.2. EGNOS

EGNOS results from this study showed: (i) short-term static and guidance RMS errors below 60 cm, (ii) long-term static and guidance RMS errors in the 1–2 m range, and (iii) improvements of up to approximately 41% compared with unaugmented (*Section 3.3.2*). The positioning errors obtained in this study are approximately consistent with the positioning errors announced by government agencies, for example: (i) the European GNSS Agency states that EGNOS is expected to provide a minimum horizontal accuracy of 3 m R95 (EGNSS Agency, 2025), and (ii) tests conducted by the European Union Agency for the Space Program in April 2025 in 28 European locations reported errors between 0.8 and 1.9 m R95. Our positioning errors are also consistent with the literature, for example: (i) according to some books, under good conditions, EGNOS can achieve a positioning error of around 1 m (Shannon et al., 2018; Walter, 2020); and (ii) positioning errors consistently less than 1.3 m using EGNOS were reported, while GPS alone yielded errors of up to 3 m (Tabti, 2025). Our guidance errors are also consistent with other studies applying EGNOS in tractor guidance, reporting short-term pass-to-pass errors of 0.2 m R95 (Vázquez et al., 2019) and 0.25 m median (Radočaj et al., 2022). Overall, our results, reports from government agencies, and results from other researchers indicate that EGNOS positioning typically results in short-term guidance RMS errors below 60 cm, which increase to 1–2 m in the long term, representing an improvement of approximately 41% compared to unaugmented GNSS.

#### 4.1.3. GLIDE

GLIDE results from this study showed: (i) short-term static and guidance RMS errors below 20 cm, and (ii) no improvement in the long term (*Section 3.3.3*). The short-term guidance error obtained in this study with GLIDE falls well within the 20 cm threshold specified in the GLIDE datasheets, which indicate pass-to-pass precision within 20 cm over a 15-minute interval (Novatel, 2015). Furthermore, Fig. B.5c closely resembles the pass-to-pass error graphs in the datasheets, corresponding to intervals of 1, 10, 50, 100, 300, 600, and 900 seconds, and clearly illustrates a similar upward trend over time (Novatel, 2015). A literature review found only one prior study evaluating GLIDE in tractor guidance, which reported a guidance error of 9 cm for a 15-minute interval (Guzman et al., 2016), confirming the GLIDE specifications. Overall, our results, technical datasheets, and results from other researchers indicate that Novatel's GLIDE technology achieves short-term guidance RMS errors below a 20 cm threshold when the time between passes does not exceed 15 minutes, with this threshold increasing at longer intervals, while it does not provide improvements in long-term guidance.

#### 4.1.4. RTK

Baseline length influenced the accuracy in single-base RTK mode, as evidenced by the results of configurations C8–C12 and C14, with base stations located at distances of 645, 296, 100, 42, 14, and 0 km, which yielded RMS positioning errors below 10 mm plus 1 mm per kilometre of baseline, in compliance with the specifications stated by the manufacturer of this receiver (*Section 3.3.4*). This is similar to the accuracy of other RTK GNSS receivers such as Trimble R750 (8 mm + 1 ppm), Topcon AGS-2 (10 mm + 1 ppm), and Leica mojoXact Plus (10 mm + 1 ppm). Scientific studies have described a reduction in RTK GNSS accuracy as baseline length increases (Grejner-Brzezinska et al., 2005; Mahato et al., 2024b; Wang et al., 2022). Overall, considering our measured errors for the Harxon TS108PRO, its specifications, those of other receivers, and information from related studies, it can be concluded that receivers working in RTK mode generally achieve an RMS positioning error not exceeding 1 cm plus 1 mm per kilometre of baseline.

Long-baseline RTK results from this study, with baselines exceeding 100 km, showed positioning RMS errors in the 1.4–73.3 cm range and guidance RMS errors in the 17.3–83.5 cm range (*Section 3.3.4*).

Literature reports similar positioning errors for long baselines: 5.2 cm and 8.7 cm for a baseline of 103 km (Wang and Yu, 2024); 10 cm SD for a baseline of 109 km (Li et al., 2018); SDs of 3.1–14.2 cm SD error for 112–120 km baselines (Hou et al., 2020); and errors of a few centimetres for baselines spanning hundreds of kilometres (Grejner-Brzezinska et al., 2005). No tractor guidance studies were found for long baselines. Overall, our results, the specifications of the Harxon TS108PRO, and the positioning errors reported in other scientific studies with long baselines, suggest that long-baseline RTK over 100 km typically achieves guidance RMS errors exceeding 17 cm and, in most cases, substantially higher.

Medium-baseline RTK results from this study, with baselines between 20 and 100 km, showed static RMS errors in the 0.8–9.4 cm range and guidance RMS errors in the 2.8–19.6 cm range (*Section 3.3.4*). Literature reports similar positioning errors for baselines of 22 km (SD 1.5 cm) (Li et al., 2018), 30 km (1.29–2.26 cm) and 43 km (1.6–5.6 cm) (Gökdaş and Özlüdemir, 2020), 56 km (SD 1.8–2.0 cm) (Hou et al., 2020), and 67 km (RMS 20 cm) (Kowalczyk and Hadas, 2024). Overall, our results, the specifications of the Harxon TS108PRO, and the positioning and guidance errors for medium-baselines reported in other studies, suggest that medium-baseline RTK, with baselines between 20 and 100 km, typically achieves guidance RMS errors within or close to the 3–20 cm range.

Short-baseline RTK results from this study, conducted with a baseline shorter than 20 km, showed positioning RMS errors ranging from 0.6 to 1.2 cm, and guidance RMS errors ranging from 2.3 to 2.5 cm (*Section 3.3.4*). Literature reports similar positioning errors for baselines of 20 m (SD <1 cm) (Pan et al., 2022), 1–10 km (SDs 1–4 cm) (Dabove, 2019), 1.6–5 km (RMS 0.47–1.05 cm) (Gökdaş and Özlüdemir, 2020), 9 km (0.5–0.8 cm) (Wang and Yu, 2024), and 3–6 km (SD 1 cm) (Wang et al., 2022). Similar guidance errors have been found with baselines of 300 m (2.4 cm) (Carballido et al., 2014), 2.5 km (RMS < 2.5 cm) (Zhang et al., 2021), and 18 km (mean < 3 cm) (Radočaj et al., 2022). Literature additionally shows larger errors (30–80 cm), attributable to the use of low-cost receivers and environments with reduced satellite visibility (Mahato et al., 2020; Mishra et al., 2024). Overall, our results, the specifications of the Harxon TS108PRO, and positioning and guidance errors for short baselines reported in other studies suggest that short-baseline RTK, corresponding to baselines shorter than 20 km, typically achieves guidance RMS errors in the 2–3 cm range.

Position solutions in RTK mode from our study were float or DGNSS for long baselines, fixed or float for medium baselines, and fixed for short baselines (*Section 3.3.4*). A fixed solution occurs when the RTK receiver has successfully resolved the integer ambiguities of the carrier phase measurements, providing centimetre-level accuracy, typically around 1–2 cm. A float solution occurs when the RTK receiver cannot resolve the ambiguities considering an integer number of carrier phase cycles, and resolves it with a float number of phase cycles, providing decimetre-level accuracy of 10–30 cm. A DGNSS solution is provided by RTK receivers when neither a fixed nor a float solution can be achieved. It is crucial that both rover and base see the same satellites to resolve ambiguities and obtain a fixed, or at least a float solution (Leick et al., 2015). As the baseline increases, the number of common-view satellites decreases, making it more difficult to obtain a fixed solution. Studies in the literature report this behaviour, for example: when the baseline increases, atmospheric residual errors also increase, reducing the accuracy of the float solution and decreasing the ambiguity resolution ratio (Wang et al., 2022); fixed solutions were achieved 97%–99% of the time with baselines between 45 and 66 km (Dang et al., 2023); float solutions were found for baselines between 40 and 200 km (Jensen and Cannon, 2000); fixed solutions were obtained nearly 100% of the time with baselines between 1.6 and 42.8 km (Gökdaş and Özlüdemir, 2020); position solution depends on the distance to the base, but also on the quality of the receiver and GNSS antenna (Mahato et al., 2025). Overall, our results and the analysed literature suggest that RTK positioning typically provides float or DGNSS solutions for long baselines, fixed or float solutions for medium baselines, and fixed solutions for short baselines.

#### 4.1.5. VRS-NRTK

VRS-NRTK results showed a mean improvement of about 17% over single-base, short-baseline RTK, with guidance RMS errors in the 1.4–1.6 cm range (*Section 3.3.5*). Studies comparing VRS-NRTK with single-base RTK positioning also found improvements, such as reductions in geometric and tropospheric errors (Vollath et al., 2002), a 2-cm smaller error on a 3 km baseline (Dabove, 2019), and faster initialisation times under low satellite visibility (Sun and Gibbings, 2005). No tractor guidance studies evaluating VRS-NRTK were found. Overall, our results and previous studies suggest that VRS-NRTK is preferable to single-base RTK for short baselines, with error reductions of about 17% and guidance RMS errors within the 1–2 cm range.

#### 4.1.6. On-site RTK

On-site RTK results from this study showed the highest accuracy, with positioning RMS errors in the 0.3–0.4 cm range and guidance RMS errors in the 1.2–1.3 cm range (*Section 3.3.6*). Literature reports similar positioning errors with low-cost receivers (RMS 5.5 mm) (Garrido-Carretero et al., 2019), GPS-only and GPS/IRNSS RTK (<1 cm) (Pan et al., 2022), multi-frequency Galileo RTK (RMS 1 mm) (Tu et al., 2019), and RTK-BDS-3 (mean 8.9 mm) (Zhang et al., 2020). Similar tractor guidance errors have been found including 2.4 cm (Carballido et al., 2014), 4.5 cm (Kowalczyk and Hadas, 2024), 1 cm (Li et al., 2021), 2 cm (Sun et al., 2010), 5 cm (Takai et al., 2014), and <6 cm (Yin et al., 2020). Overall, our results and previous studies show that on-site RTK provides the highest accuracy, with guidance errors close to 1 cm for both short- and long-term applications.

#### 4.1.7. Summary of findings

Overall, the previous findings, together with information from Table 4 and Fig. 16, can be summarised as follows:

(i) Unaugmented GNSS positioning typically results in long-term guidance RMS errors of 2–3 m, and short-term guidance RMS errors below 1 m, with variations of around 50% depending on receiver quality; (ii) EGNOS positioning typically results in short-term guidance RMS errors below 60 cm, which increase to 1–2 m in the long term, representing an improvement of approximately 41% compared to unaugmented GNSS; (iii) GLIDE technology achieves short-term guidance RMS errors below a 20 cm threshold when the time between passes does not exceed 15 minutes, with this threshold increasing at longer intervals, while it does not provide improvements in long-term guidance; (iv) RTK generally achieves positioning RMS errors not exceeding 1 cm plus 1 mm per kilometre of baseline; (v) Long-baseline RTK over 100 km achieves guidance RMS errors exceeding 17 cm and in most cases substantially higher; (vi) Medium-baseline RTK, with baselines between 20 and 100 km, achieves guidance RMS errors within or close to the 3–20 cm range; (vii) Short-baseline RTK, corresponding to baselines shorter than 20 km, achieves guidance RMS errors in the 2–3 cm range; (viii) RTK positioning typically provides float or DGNSS solutions for long baselines, fixed or float solutions for medium baselines, and fixed solutions for short baselines; (ix) VRS-NRTK is preferable to single-base RTK for short baselines, with error reductions of about 17% and guidance RMS errors within the 1-2 cm range; and (x) On-site RTK provides the highest accuracy for short- and long-term applications, with guidance errors close to 1 cm.

#### 4.1.8. Recommendations for selecting guidance technologies

Based on the findings discussed above, four main technology options for farmers can be identified, relying on the authors' knowledge of cereal agriculture in Spain.

- EGNOS may be suitable for small-scale farmers with limited budgets, offering moderate accuracy for guidance or assisted guidance in fertilisation tasks.
- "GLIDE may be considered an appropriate option for farmers able to invest slightly more than in the previous case and working on small parcels where the time between consecutive passes is short. It provides sufficient accuracy for guidance in fertilisation, spraying, and field preparation tasks. In addition, it stands out for its simplicity, as it requires neither Internet connectivity nor network registration."
- VRS-NRTK may be considered for farmers with free access to an NRTK and working in areas with Internet connectivity. It provides adequate accuracy for guidance in all farming tasks. This option stands out for offering the best value-for-money.
- On-site RTK may be considered an appropriate option for farmers who lack NRTK coverage in their region, do not have Internet connectivity in their fields, or have specific high-precision requirements. However, this option is constrained by the need to deploy a reference base close to the plot.

These recommendations underline the importance of considering both technical performance and practical constraints when selecting a guidance solution. Economic factors, infrastructure availability, and farm-specific conditions play a decisive role in determining whether a given technology can be effectively adopted in real farming operations.

### 4.2. Strenghts, limitations, and future research

Many studies evaluate GNSS receivers and augmentation systems for tractor guidance, but they usually focus on a single type of receiver and a single augmentation system. This study is the first to assess three categories of GNSS receivers, low-cost, mid-range, and high-end, together with five types of augmentation under the same experimental conditions. This represents the main novelty of the study, which has been broken down into eight strengths: (i) It evaluates positioning options available to farmers that typically do not require subscription fees, emphasizing solutions that are expected to be more economically efficient over time. Other studies evaluate guidance systems that require subscription quotes (Carballido et al., 2014; Kowalczyk and Hadas, 2024; Yin et al., 2020). (ii) It offers an extensive assessment of five no-fee GNSS augmentation systems, including EGNOS, RTK, VRS-NRTK, on-site RTK, and the proprietary Novatel GLIDE technology, under realistic agricultural conditions. To our knowledge, no existing publication provides an equivalent comparative analysis, since most similar studies test only a single GNSS solution (Nguyen et al., 2021; Nguyen and Cho, 2023; Vázquez et al., 2019; Zhang et al., 2021). (iii) It evaluates 14 different receiver-augmentation combinations, an unprecedented number in the literature, including low-cost, mid-range, and high-end GNSS receivers. Other studies assess a small number of combinations, such as three (Alkan et al., 2020), four (Guzman et al., 2016), two (Pan et al., 2022), and nine (Sun et al., 2017). (iv) It includes static positioning tests and realistic tractor guidance tests, whereas other studies rely only on static positioning (Garrido-Carretero et al., 2019; Tu et al., 2019; Zhang et al., 2020) or guidance tests (Kowalczyk and Hadas, 2024; Rounsaville et al., 2016; Zhang et al., 2021). (v) It provides performance results for both short-term and long-term periods, whereas most previous studies have focused solely on the short term (Carballido et al., 2014; Rounsaville et al., 2016; Vázquez et al., 2019). (vi) It reports error metrics using six statistical indicators (RMS, mean error, SD, CEP, R95, and R997), enhancing comparability across studies, whereas most previous works rely on a single metric (Alkan et al., 2020; Karimi, 2021; Nguyen et al., 2021; Zhang et al., 2021; Zhang and Pan, 2022). (vii) It investigates the effect of baseline length, extending to unusually long distances of up to 645 km. Although previous works have studied the influence of baseline length under static conditions, its role in real tractor guidance remains unexplored (Gökdaş and Özlüdemir, 2020; Shi et al., 2020; Wang and Yu, 2024). (viii) It provides a link to the dataset in an open-access repository, which was not done in any of the reviewed studies.

Three limitations are present in this study. First, the execution of the guidance tests was conducted consecutively rather than in parallel, resulting in different satellite geometry for each test. Nevertheless, the static tests were conducted in parallel and provided sufficient accuracy information for each tested configuration. Moreover, overcoming this limitation would have required 14 tractors performing guidance simultaneously, greatly increasing the necessary equipment and complicating the testing logistics. Second, the long-term guidance errors were estimated using error values from short- and long-term static positioning tests, combined with error values from short-term guidance tests. Overcoming this limitation would have required a very large number of guidance tests, evenly spaced over days, weeks, or months, which would have greatly complicated the experiment's logistics. Moreover, the static test provides sufficient information to estimate long-term guidance behaviour, and the resulting long-term error estimation is based on a solid foundation. Finally, tests were conducted under specific experimental conditions, including a particular latitude, flat and unobstructed fields with full satellite visibility, stable atmospheric conditions, satellite geometries corresponding to the test days, specific GNSS receiver models, and straight-line guidance at a speed of 1 m/s. Despite this, we consider that the results are representative of the GNSS receiver category and augmentation technique assessed.

An important line of future research would be to assess a range of PPP correction services, including the recently introduced and freely available Galileo High Accuracy Service (HAS), as well as commercial, subscription-based solutions such as John Deere's StarFire, Trimble's RTX, and Novatel's TerraStar. The proprietary nature of these three latter services may complicate their integration into open guidance platforms, but their inclusion would enable a more complete comparison of the performance of unaugmented, PPP, and RTK positioning technologies.

## 5. Conclusions

In summary, the comparison of several GNSS augmentation technologies, through static tests and guidance tests using a tractor along a straight trajectory under identical methodological conditions, demonstrated that: unaugmented GNSS resulted in guidance errors of 2–3 m, reduced below 1 m in pass-to-pass intervals shorter than 15 minutes; EGNOS reduced these guidance errors by ~41%; GLIDE reduced guidance errors to below 20 cm for pass-to-pass intervals shorter than 15 minutes, with no long-term improvement; RTK guidance error decreased as baseline length shortened: >100 km yielded >17 cm, 20–100 km yielded 3–20 cm, and <20 km yielded 2–3 cm; VRS-NRTK slightly outperformed RTK with similar baseline lengths; and on-site RTK enabled 1 cm guidance error. Overall, low-cost receivers without augmentation or with EGNOS result in metre-level errors; mid-range receivers with GLIDE deliver decimetre-level guidance errors in the short term; and high-end receivers using on-site RTK or VRS-NRTK on baselines up to 100 km achieve centimetre-level errors, enabling farmers to replicate tractor trajectories consistently year to year.

## CRediT authorship contribution statement

**Jaime Gomez-Gil:** Writing – review & editing, Writing – original draft, Validation, Supervision, Project administration, Methodology, Formal analysis, Conceptualization. **Angel Alonso-Garcia:** Writing – review & editing, Visualization, Software, Methodology, Investigation, Data curation, Conceptualization. **Sergio Alonso-Garcia:** Writing – review & editing, Software, Resources. **Fco. Javier Gomez-Gil:** Writing – review & editing, Writing – original draft, Formal analysis, Conceptualization.

## Declaration of competing interest

The authors declare that they have no known competing financial interests or personal relationships that could have appeared to influence the work reported in this paper.

## Acknowledgments

The authors would like to express their sincere gratitude to the TractorDrive company (www.tractordrive.es) for their generous support, including the provision of GNSS receivers, an automatic tractor guidance system, and their valuable technical expertise, which greatly contributed to this study. The authors also wish to thank Cesar Domínguez from the Ingeniería y Sistemas Cerea company (www.cereagps.com) for sharing his knowledge, which has been instrumental in shaping key aspects of this work. Special thanks are extended to David Nafría, from the Instituto Tecnológico Agrario de Castilla y León (www.itacyl.es), and to Manuel Serna Puente, from the Instituto Geográfico Nacional (www.ign.es), for their support in accessing and utilising the NRTK correction service. Special thanks are extended to César Gutiérrez, mathematician and full professor at the University of Valladolid, for his thorough review of the statistical components of this study and for his valuable guidance.

The research was partially supported by the project PID2021-125080OB-I00, funded by the Spanish Ministry of Science and Innovation. It was also partially supported by the project TED2021-131551B-I00, funded by MCIN/AEl/10.13039/501100011033 and the European Union "NextGenerationEU/PRTR".

## Appendix A. GNSS hardware and messaging

### A.1. Positioning receivers

This study tested the performance of three positioning receivers:

- **Navilock NL8022MP.** This is a low-cost code GNSS receiver that offers SPP and processes L1 signals in the GPS system, E1 signals in the Galileo system, L1 signals in the GLONASS system, B1 signals in the BeiDou system, and L1 signals in the QZSS (Quasi-Zenith Satellite System). It uses a U-blox chipset and provides output positioning rates up to 10 Hz. It is compatible with Satellite-Based Augmentation Systems (SBAS). According to its datasheet, it provides horizontal accuracies of 2.5 m CEP and 2 m CEP with SBAS. The retail price of this receiver was approximately €140 in Spain in 2024. The receiver used had firmware version 3.01. The U-Center 22.07 application was used to configure the baud rate of the serial connection and the positioning update rate, to activate or deactivate SBAS, and to select the RMC and GGA sentences.
- **Novatel Smart2.** This is a mid-range GNSS receiver supporting carrier-phase measurements, and capable of processing L1, L2, and L2C signals in the GPS system; L1 signals in the SBAS system; E1 and E5b signals in the Galileo system; L1 and L2 signals in the GLONASS system; B1I, B2I, and B2b in the BeiDou system; and L1 and L2 in the QZSS system. It uses a Hexagon/Novatel OEM chipset and offers output positioning rates of up to 20 Hz. It is compatible with SBAS and the PPP technique provided by the TerraStar company. According to its datasheet, it offers horizontal accuracies of 1.5 m RMS in L1 positioning, 1.2 m RMS in L1/L2 positioning, 60 cm RMS in L1/L2 positioning with SBAS, 40 cm with a subscription to TerraStar-L PPP service, and 2 cm with a subscription to the TerraStar-C PRO PPP service. This receiver also has a special technology called GLIDE, which reduces the relative pass-to-pass error in agricultural tasks. The retail price of this receiver was approximately €1000 in Spain in 2024. The receiver used had firmware version 7.08.01. The Tera Term 4.104 application was used to configure the baud rate of the serial connection and the positioning update rate, to activate or deactivate SBAS, to activate or deactivate GLIDE, and to select the RMC and GGA sentences.
- **Harxon TS108PRO.** This is a high-end RTK GNSS receiver supporting carrier-phase measurements and capable of processing L1, L2, and L5 signals in the GPS system; E1, E5a, and E5b signals in the Galileo system; L1 and L2 signals in the GLONASS system; and B1, B2, and B3 signals in the BeiDou system. It is compatible with SBAS. It uses an UM4B0 Unicore chipset and offers output positioning rates of up to 10 Hz. According to its datasheet, it offers horizontal accuracies of 1.5 m RMS in single-point positioning and 1 cm in RTK positioning. The retail price of this receiver was approximately €2000 in Spain in 2024. The receiver used had firmware version V003.01.22. The Harxon Smart Tool 1.3.1 application was used to configure the baud rate of the serial connection and the positioning update rate, to select the correction source from SBAS, radio link, or Bluetooth, and to select the RMC and GGA sentences. Lefebure NTRIP Client 2021.12.03 was used to configure and receive corrections from the NRTK used and send them to the receiver via Bluetooth.

In order to obtain a reference positioning, a Harxon TS103 base was used. This is a high-performance RTK GNSS base capable of processing L1, L2 and L5 signals in the GPS system, E1, E5a and E5b signals in Galileo system, L1 and L2 signals in GLONASS system, and B1, B2 and B3 signals in the BeiDou system. It uses an UM4B0 Unicore chipset, and offers output positioning rates up to 10 Hz. According to its datasheet, it offers code measurement precision of 10 cm and carrier phase measurement precision of 1 mm. The retail price of this receiver was approximately €1500 in Spain in 2024.

### A.2. Obtention of information of GNSS receivers

The positioning information of GNSS receivers in static and guidance tests was acquired from RMC and GGA sentences in the NMEA protocol.

The RMC sentences were received at a 5 Hz frequency, providing latitude and longitude in the third and fourth fields. The latitude and longitude geographic coordinates were converted to North, East, Down (NED) Cartesian coordinates.

The GGA sentences were received at frequencies that varied for each receiver, but were around 1 Hz. The *GPS Quality indicator* field of this sentence gave us information about the type of augmentation: DGNSS or SBAS when this field was 2, RTK float when this field was 5, and fixed RTK when this field was 4. The *reference station ID* field of this sentence allowed us to discern when the augmentation was DGNSS or when it was SBAS.

## Appendix B. Figures of static test results

This appendix presents the scatter plots, cumulative distribution functions, and 15-minute positioning error evolutions of the static test for each of the 14 configurations tested.

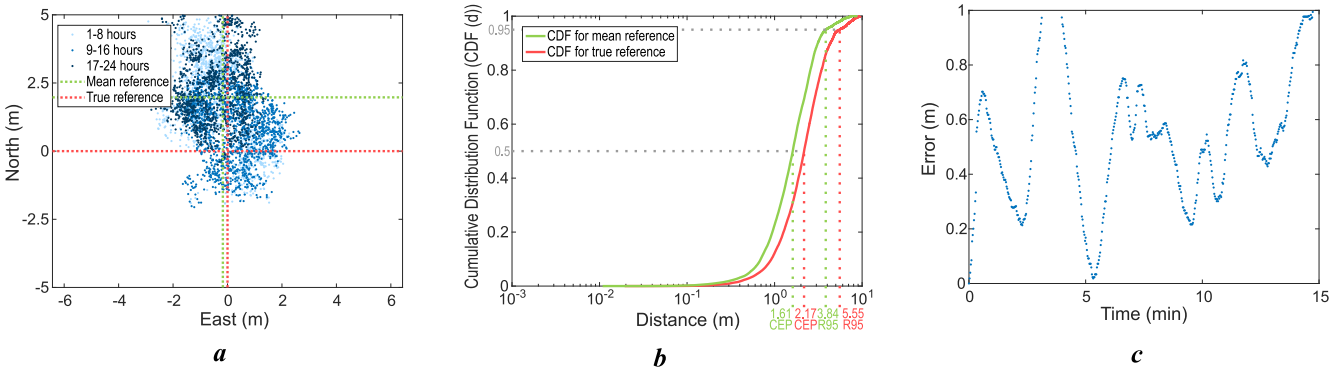


**Fig. B.1.** C1 (Navilock). Graphs obtained in the static test of the Navilock NL8022MP receiver with EGNOS off: (a) Scatter plot for 24 hours, in which 5.42% of the points are outside the limits of this plot; (b) Cumulative Distribution Function of the distances of measured positions to the mean and true reference positions from the 24-hour static tests; and (c) Evolution of the distance error with respect to the initial point, in which some points before 26 minutes, and all points after 26 minutes, are higher than 1 m, and are outside this graph.

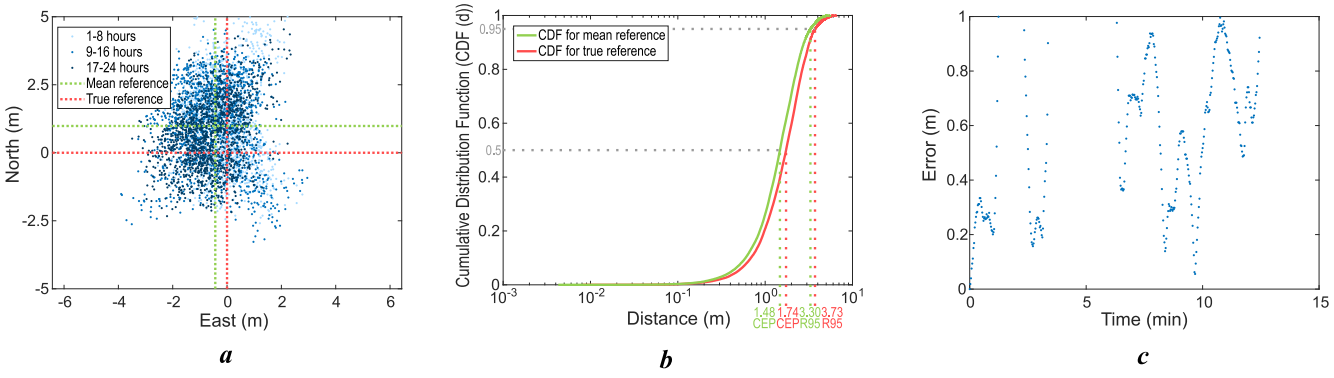


**Fig. B.2.** C2 (Navilock|EGNOS). Graphs obtained in the static test of the Navilock NL8022MP receiver with EGNOS on: (a) Scatter plot for 24 hours, in which 0.86% of the points are outside the limits of this plot; (b) Cumulative Distribution Function of the distances of measured positions to the mean and true reference positions from the 24-hour static tests; and (c) Evolution of the distance error with respect to the initial point, in which some points before 18 minutes, and all points after 18 minutes, are higher than 1 m, and are outside this graph.

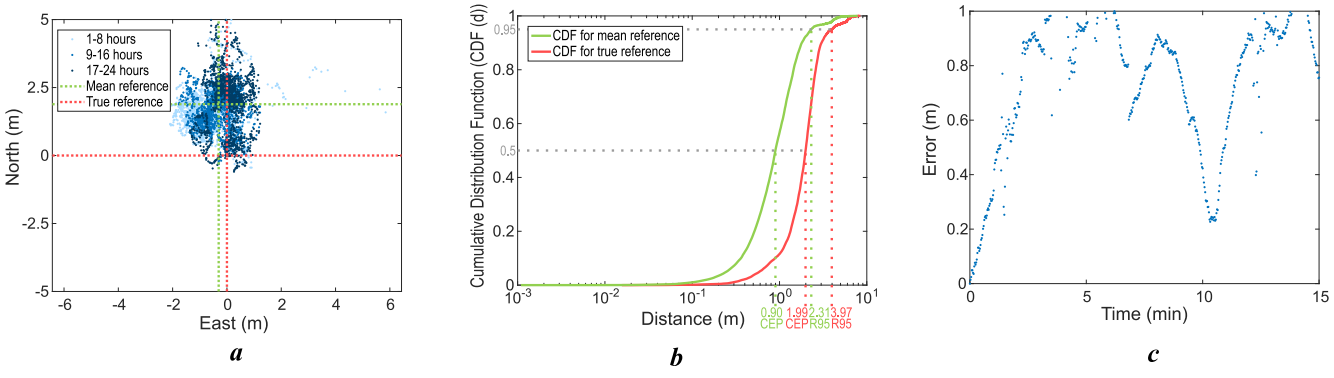


**Fig. B.3.** C3 (Novatel). Graphs obtained in the static test of the Novatel Smart2 receiver with EGNOS off and GLIDE off: (a) Scatter plot for 24 hours, in which 2.94% of the points are outside the limits of this plot; (b) Cumulative Distribution Function of the distances of measured positions to the mean and true reference positions from the 24-hour static tests; and (c) Evolution of the distance error with respect to the initial point, in which some points before 19 minutes, and all points after 19 minutes, are higher than 1 m and are outside this graph.

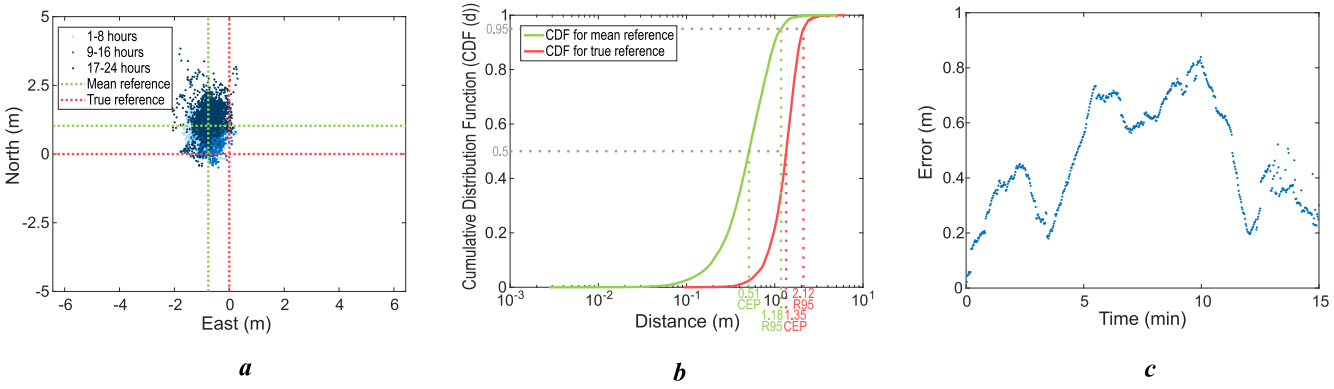


**Fig. B.4.** C4 (Novatel|EGNOS). Graphs obtained in the static test of the Novatel Smart2 receiver with EGNOS on and GLIDE off: (a) Scatter plot for 24 hours; (b) Cumulative Distribution Function of the distances of measured positions to the mean and true reference positions from the 24-hour static tests; and (c) Evolution of the distance error with respect to the initial point, in which some points are higher 1 m and are outside the graph.

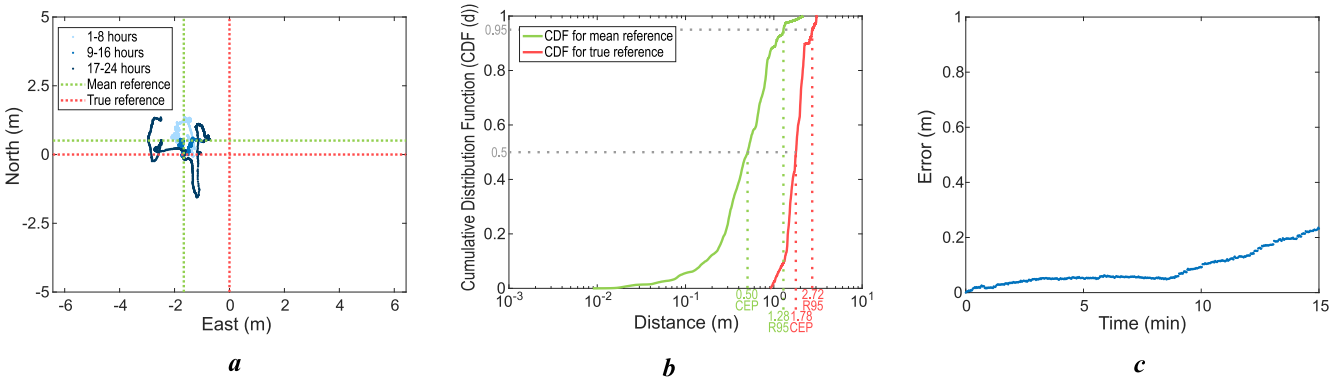


**Fig. B.5.** C5 (Novatel|EGNOS|GLIDE). Graphs obtained in the static test of the Novatel Smart2 receiver with EGNOS on and GLIDE on: (a) Scatter plot for 24 hours; (b) Cumulative Distribution Function of the distances of measured positions to the mean and true reference positions from the 24-hour static tests; and (c) Evolution of the distance error with respect to the initial point.

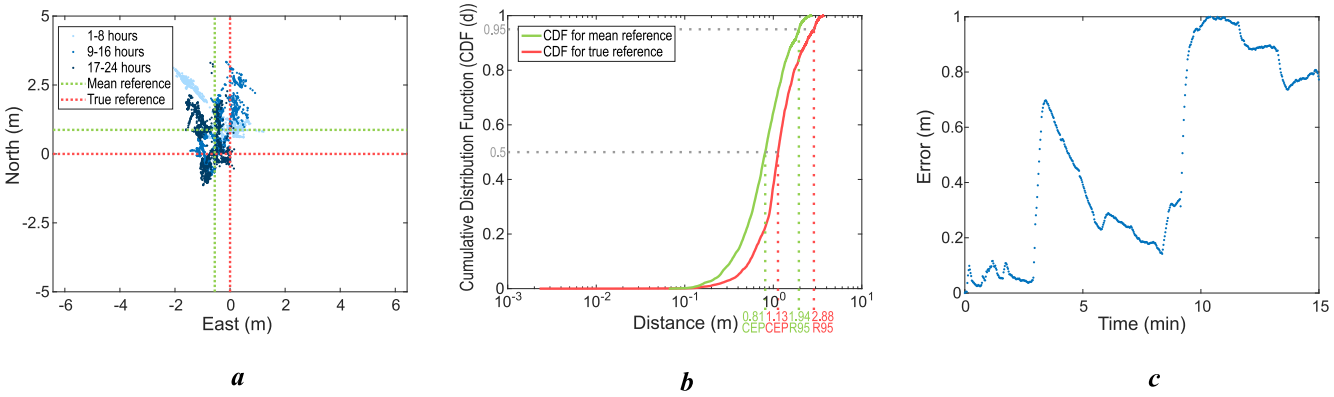


**Fig. B.6.** C6 (Harxon). Graphs obtained in the static test of the Harxon TS108PRO receiver with EGNOS off: (a) Scatter plot for 24 hours; (b) Cumulative Distribution Function of the distances of measured positions to the mean and true reference positions from the 24-hour static tests; and (c) Evolution of the distance error with respect to the initial point.

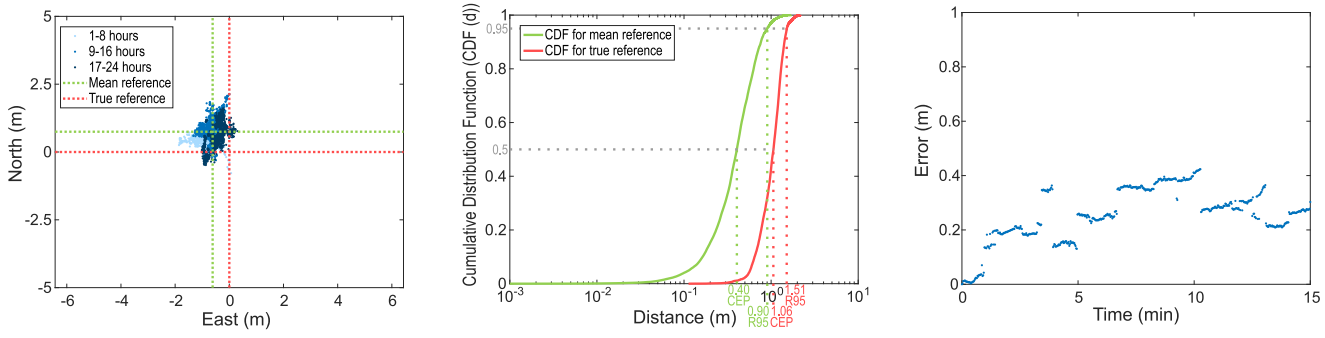


**Fig. B.7.** C7 (Harxon|EGNOS). Graphs obtained in the static test of the Harxon TS108PRO receiver with EGNOS on: (a) Scatter plot for 24 hours; (b) Cumulative Distribution Function of the distances of measured positions to the mean and true reference positions from the 24-hour static tests; and (c) Evolution of the distance error with respect to the initial point.

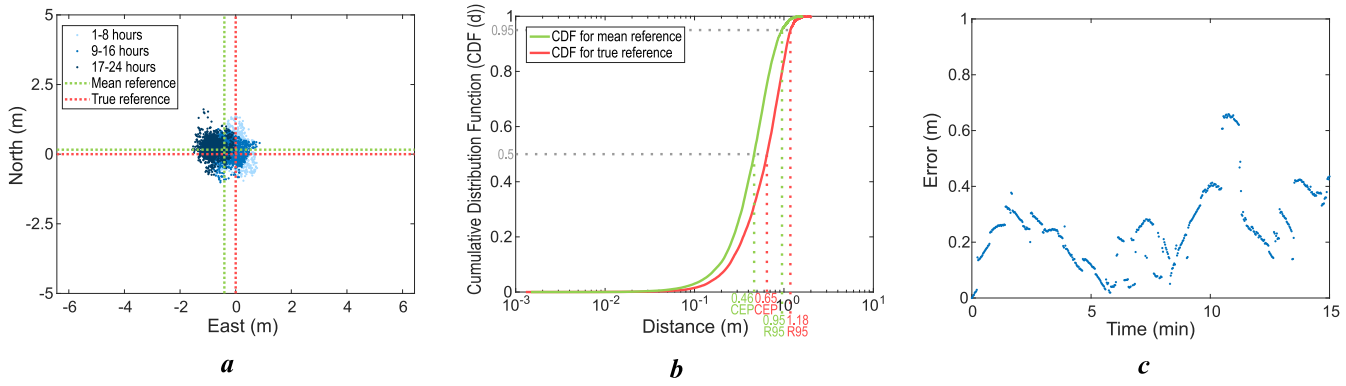


**Fig. B.8.** C8 (Harxon|RTK|645km). Graphs obtained in the static test of the Harxon TS108PRO receiver with RTK with the reference station in Girona, 645 km away from the receiver: (a) Scatter plot for 24 hours; (b) Cumulative Distribution Function of the distances of measured positions to the mean and true reference positions from the 24-hour static tests; and (c) Evolution of the distance error with respect to the initial point.

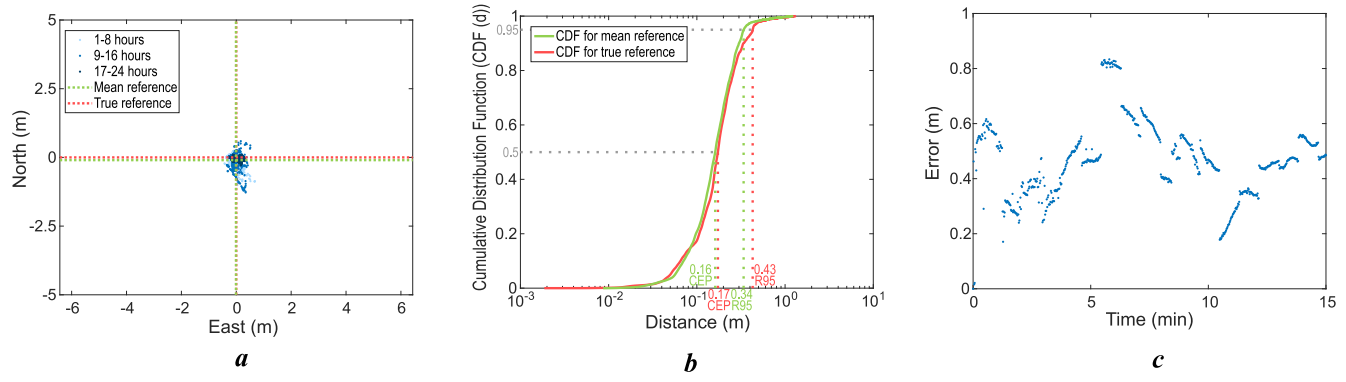


**Fig. B.9.** C9 (Harxon|RTK|296km). Graphs obtained in the static test of the Harxon TS108PRO receiver with RTK with the reference station in Mérida, 296 km away from the receiver: (a) Scatter plot for 24 hours; (b) Cumulative Distribution Function of the distances of measured positions to the mean and true reference positions from the 24-hour static tests; and (c) Evolution of the distance error with respect to the initial point.

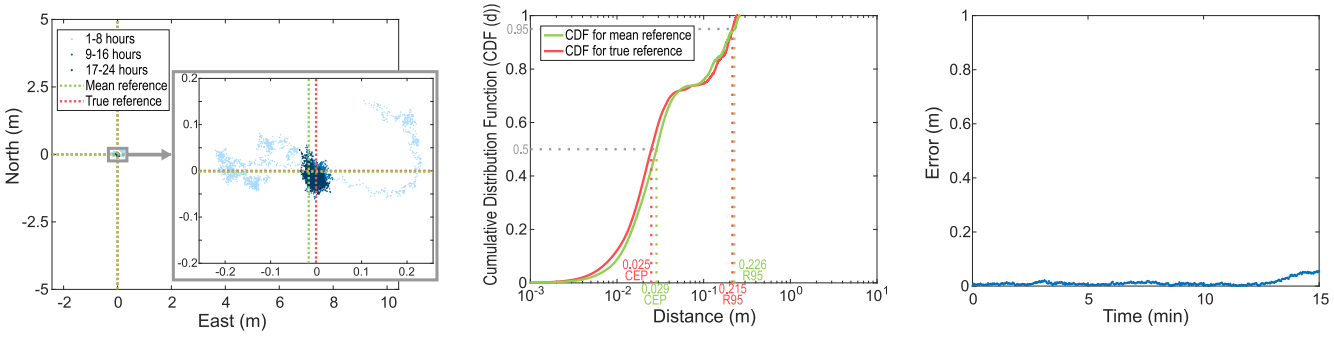


**Fig. B.10.** C10 (Harxon|RTK|100km). Graphs obtained in the static test of the Harxon TS108PRO receiver with RTK with the reference station in Aranda de Duero, 100 km away from the receiver: (a) Scatter plot for 24 hours; (b) Cumulative Distribution Function of the distances of measured positions to the mean and true reference positions from the 24-hour static tests; and (c) Evolution of the distance error with respect to the initial point.

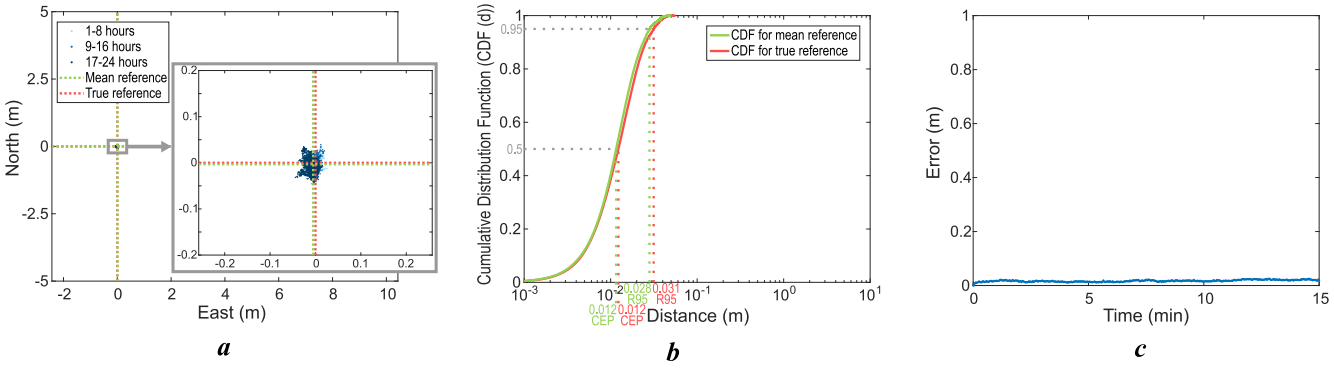


**Fig. B.11.** C11 (Harxon|RTK|42km). Graphs obtained in the static test of the Harxon TS108PRO receiver with RTK with the reference station in Valladolid, 42 km away from the receiver: (a) Scatter plot for 24 hours; (b) Cumulative Distribution Function of the distances of measured positions to the mean and true reference positions from the 24-hour static tests; and (c) Evolution of the distance error with respect to the initial point.

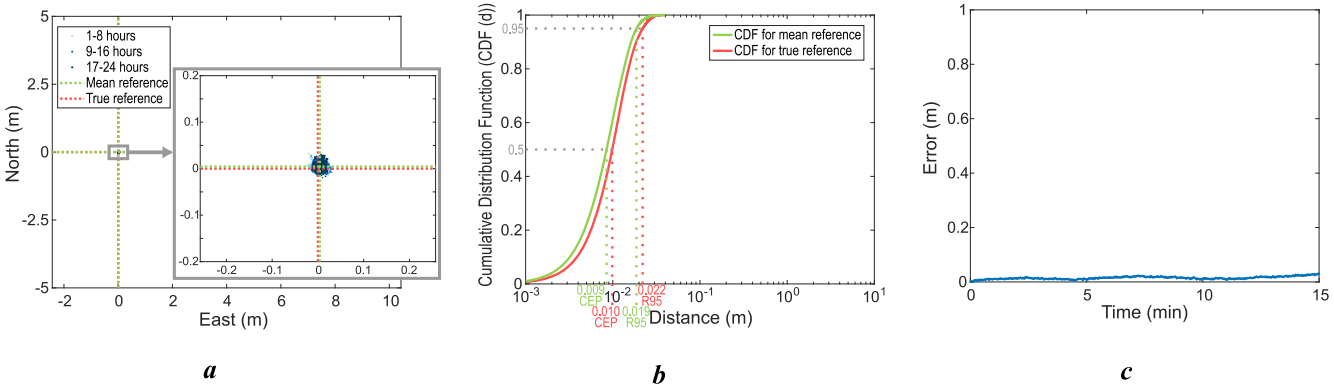


**Fig. B.12.** C12 (Harxon|RTK|14km). Graphs obtained in the static test of the Harxon TS108PRO receiver with RTK with the reference station in Olmedo, 14 km away from the receiver: (a) Scatter plot for 24 hours; (b) Cumulative Distribution Function of the distances of measured positions to the mean and true reference positions from the 24-hour static tests; and (c) Evolution of the distance error with respect to the initial point.

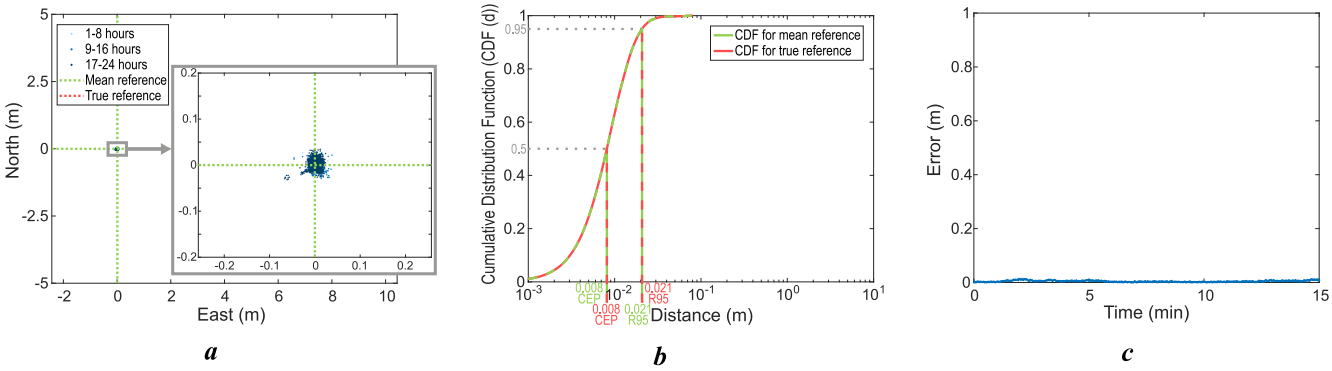


**Fig. B.13.** C13 (Harxon|VRS-NRTK|14,25,42km). Graphs obtained in the static test of the Harxon TS108PRO receiver with VRS-NRTK using a Virtual Reference Station at the receiver location: (a) Scatter plot for 24 hours, (b) Cumulative Distribution Function of the distances of measured positions to the mean and true reference positions from the 24-hour static tests; and (c) Evolution of the distance error with respect to the initial point.

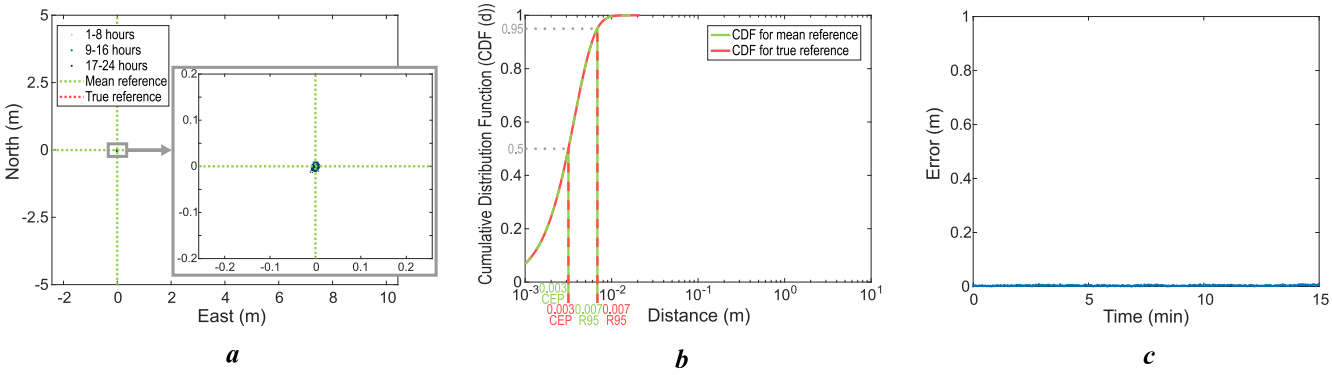


**Fig. B.14.** C14 (Harxon|On-site RTK). Graphs obtained in the static test of the Harxon TS108PRO receiver with RTK via base station located some metres from the receiver: (a) Scatter plot for 24 hours; (b) Cumulative Distribution Function of the distances of measured positions to the mean and true reference positions from the 24-hour static tests; and (c) Evolution of the distance error with respect to the initial point.

## Appendix C. Figures of guidance tests results

This appendix presents the guidance error graphs along a 300 m trajectory for each of the 14 configurations in the guidance tests.

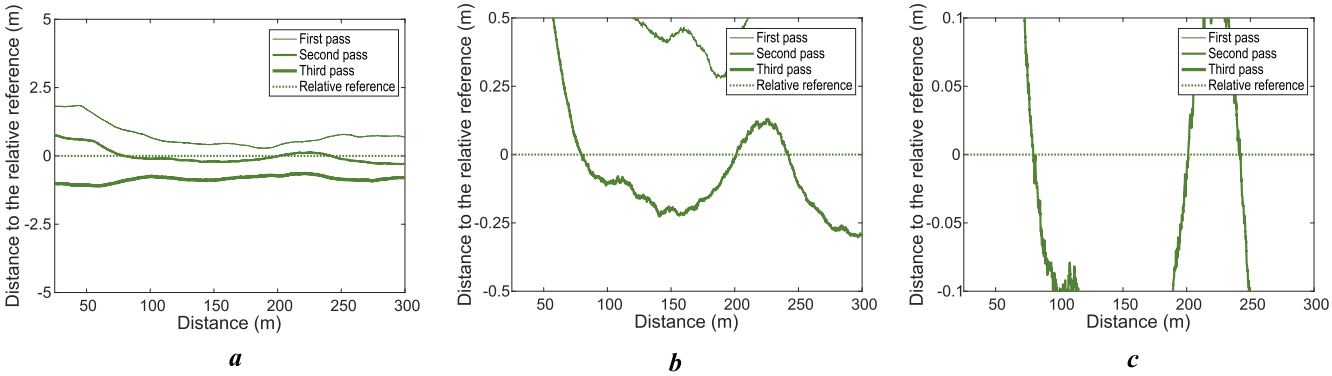


**Fig. C.1.** C1 (Navilock). Graphs showing the guidance test short-term error of the Navilock NL8022MP receiver with EGNOS off, with the ordinate axis ranging from: (a) -5 to 5 m, (b) -0.5 to 0.5 m, (c) -0.1 to 0.1 m.

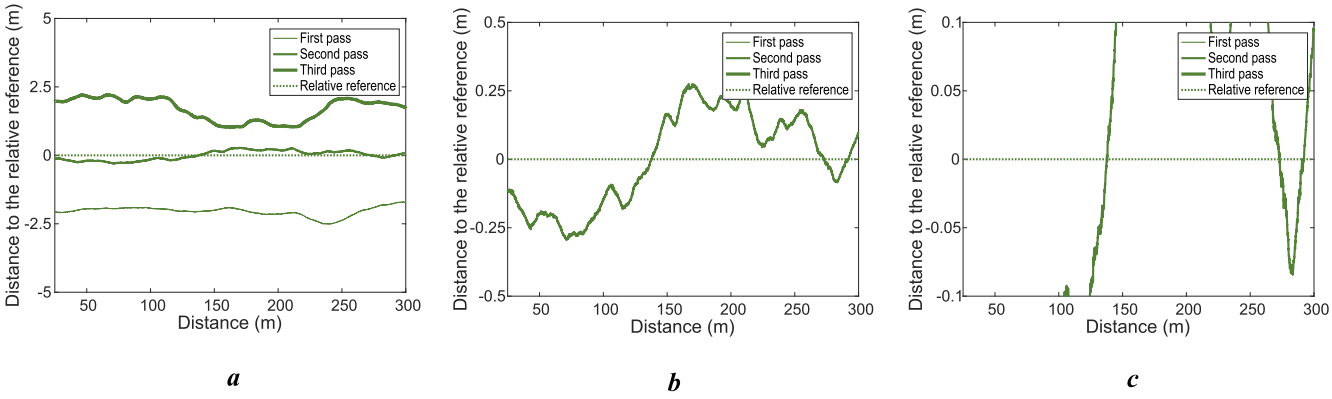


**Fig. C.2.** C2 (Navilock|EGNOS). Graphs showing the guidance test short-term error of the Navilock NL8022MP receiver with EGNOS on, with the ordinate axis ranging from: (a) -5 to 5 m, (b) -0.5 to 0.5 m, (c) -0.1 to 0.1 m.

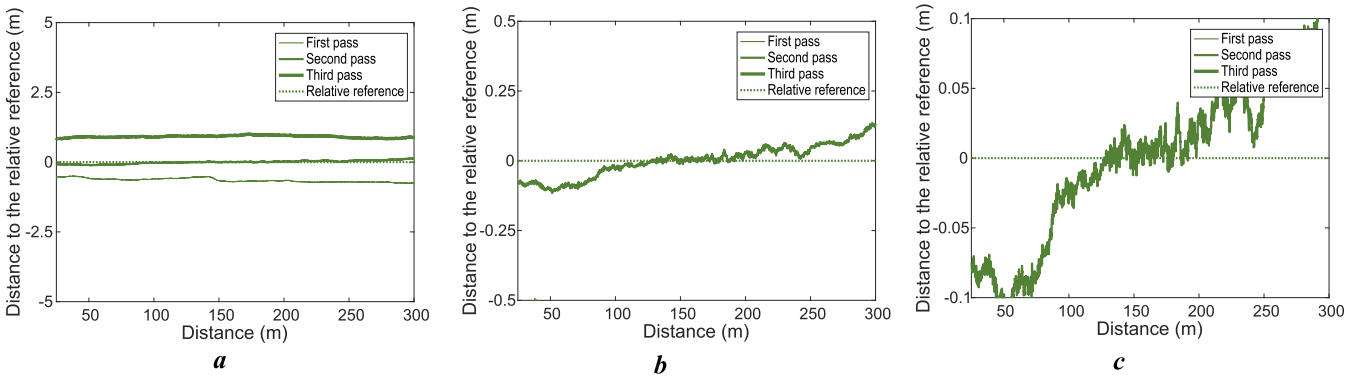


**Fig. C.3.** C3 (Novatel). Graphs showing the guidance test short-term error of the Novatel Smart2 receiver with EGNOS off and GLIDE off, with the ordinate axis ranging from: (a) -5 to 5 m, (b) -0.5 to 0.5 m, (c) -0.1 to 0.1 m.

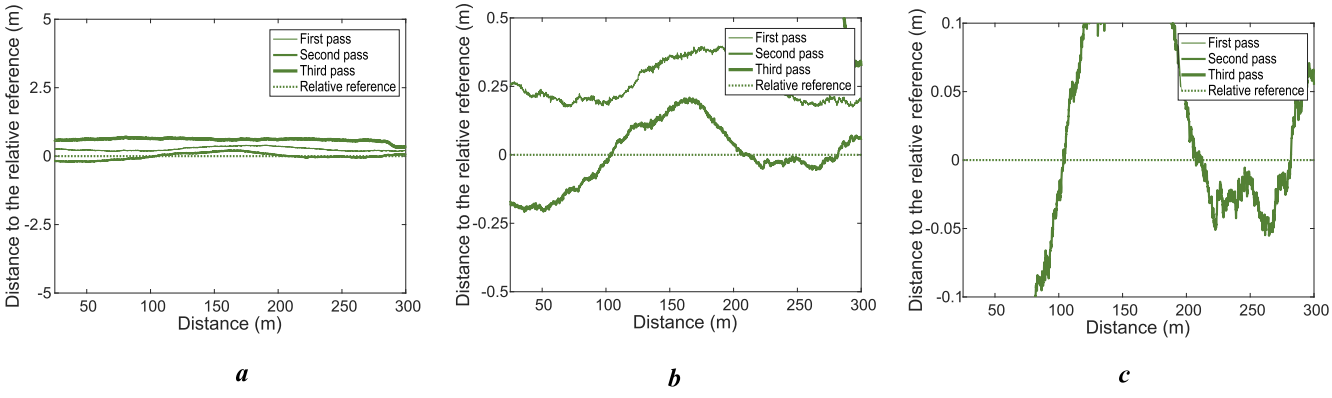


**Fig. C.4.** C4 (Novatel|EGNOS). Graphs showing the guidance test short-term error of the Novatel Smart2 receiver with EGNOS on and GLIDE off, with the ordinate axis ranging from: (a) -5 to 5 m, (b) -0.5 to 0.5 m, (c) -0.1 to 0.1 m.

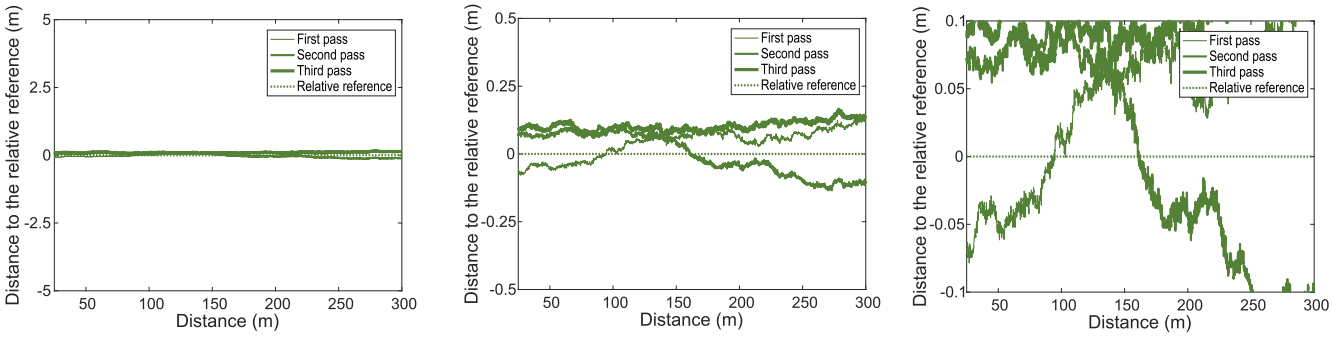


**Fig. C.5.** C5 (Novatel|EGNOS|GLIDE). Graphs showing the guidance test short-term error of the Novatel Smart2 receiver with EGNOS on and GLIDE on, with the ordinate axis ranging from: (a) -5 to 5 m, (b) -0.5 to 0.5 m, (c) -0.1 to 0.1 m.

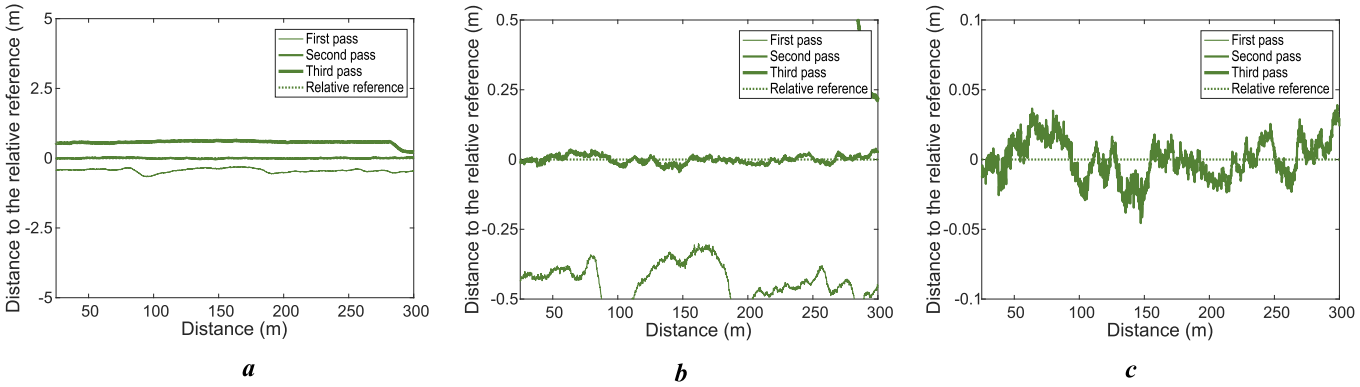


**Fig. C.6.** C6 (Harxon). Graphs showing the guidance test short-term error of the Harxon TS108PRO receiver with EGNOS off, with the ordinate axis ranging from: (a) -5 to 5 m, (b) -0.5 to 0.5 m, (c) -0.1 to 0.1 m.

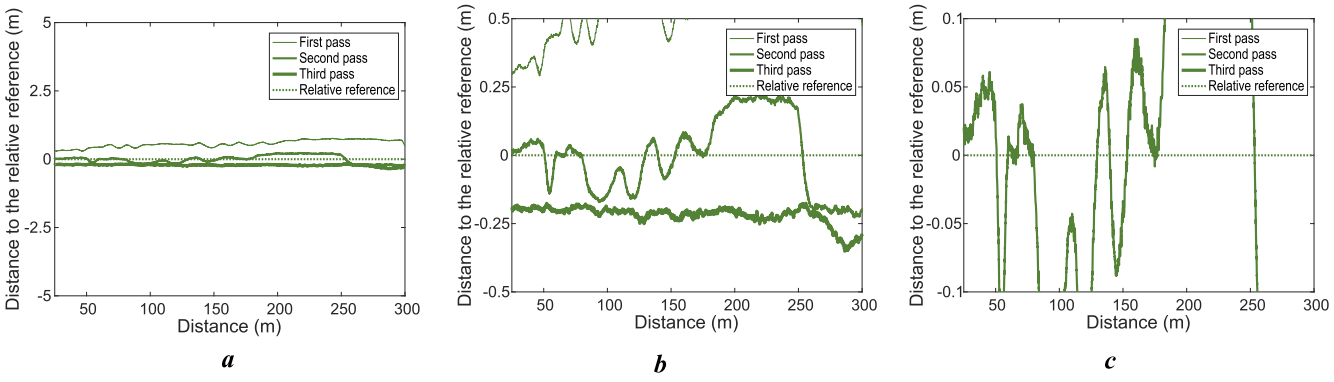


**Fig. C.7.** C7 (Harxon|EGNOS). Graphs showing the guidance test short-term error of the Harxon TS108PRO receiver with EGNOS on, with the ordinate axis ranging from: (a) -5 to 5 m, (b) -0.5 to 0.5 m, (c) -0.1 to 0.1 m.

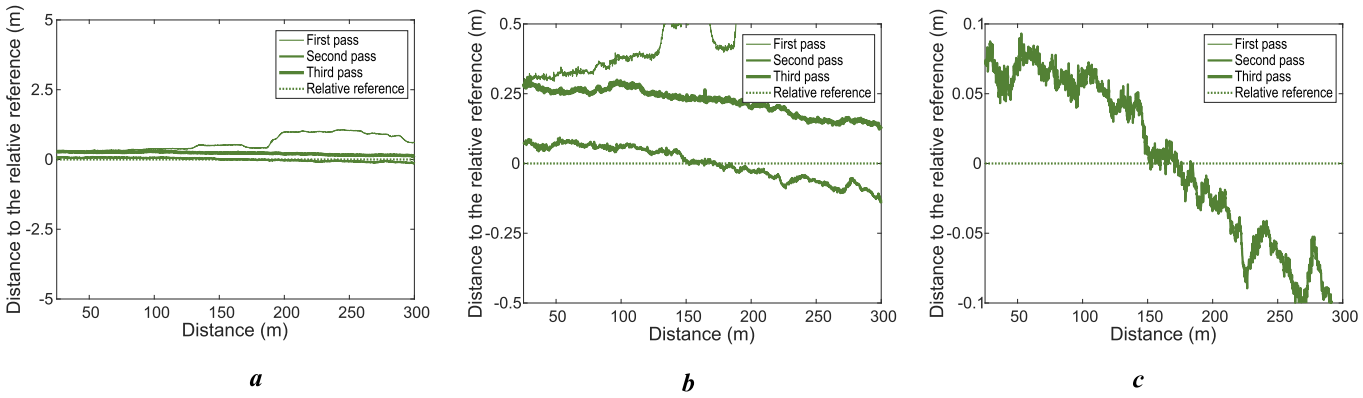


**Fig. C.8.** C8 (Harxon|RTK|645km). Graphs showing the guidance test short-term error of the Harxon TS108PRO receiver with RTK with the reference station in Girona, 645 km away from the receiver, with the ordinate axis ranging from: (a) -5 to 5 m, (b) -0.5 to 0.5 m, (c) -0.1 to 0.1 m.

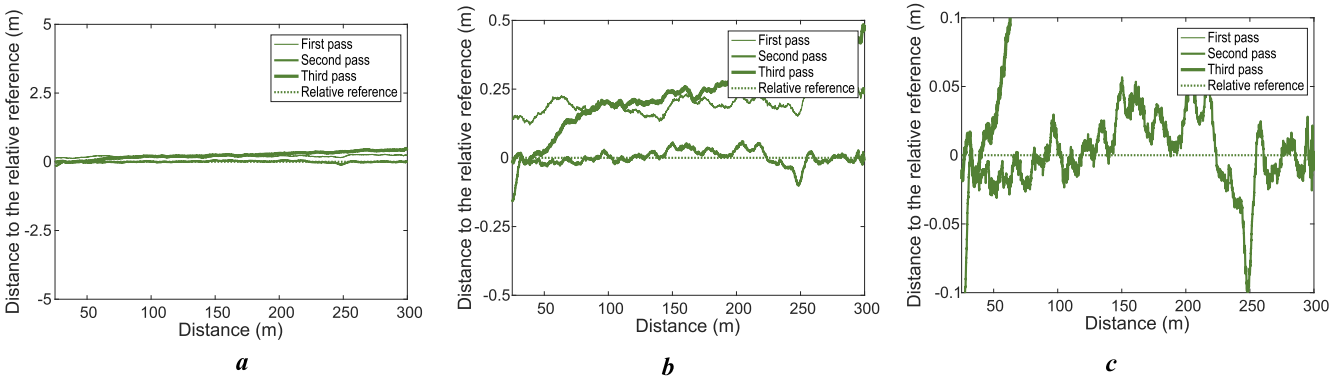


**Fig. C.9.** C9 (Harxon|RTK|296km). Graphs showing the guidance test short-term error of the Harxon TS108PRO receiver with RTK with the reference station in Mérida, 296 km away from the receiver, with the ordinate axis ranging from: (a) -5 to 5 m, (b) -0.5 to 0.5 m, (c) -0.1 to 0.1 m.

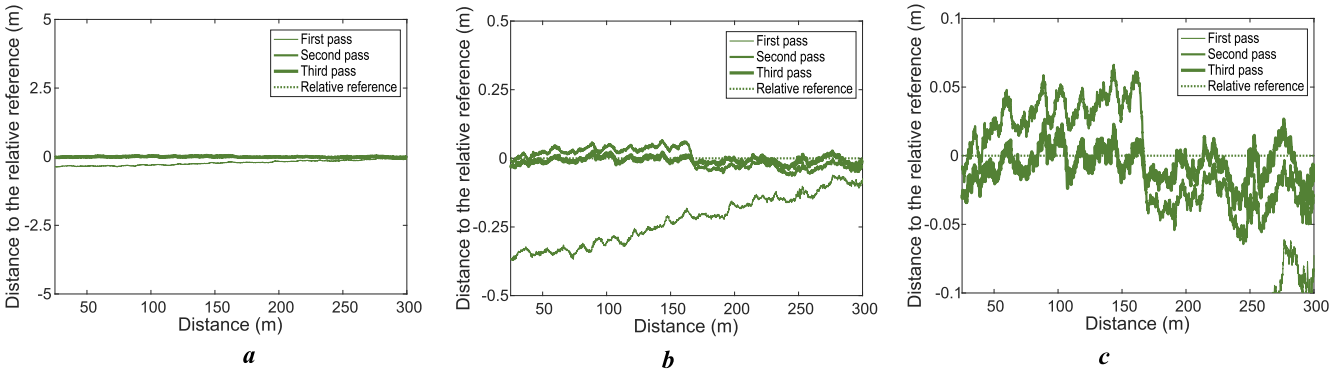


**Fig. C.10.** C10 (Harxon|RTK|100km). Graphs showing the guidance test short-term error of the Harxon TS108PRO receiver with RTK with the reference station in Aranda de Duero, 100 km away from the receiver, with the ordinate axis ranging from: (a) -5 to 5 m, (b) -0.5 to 0.5 m, (c) -0.1 to 0.1 m.

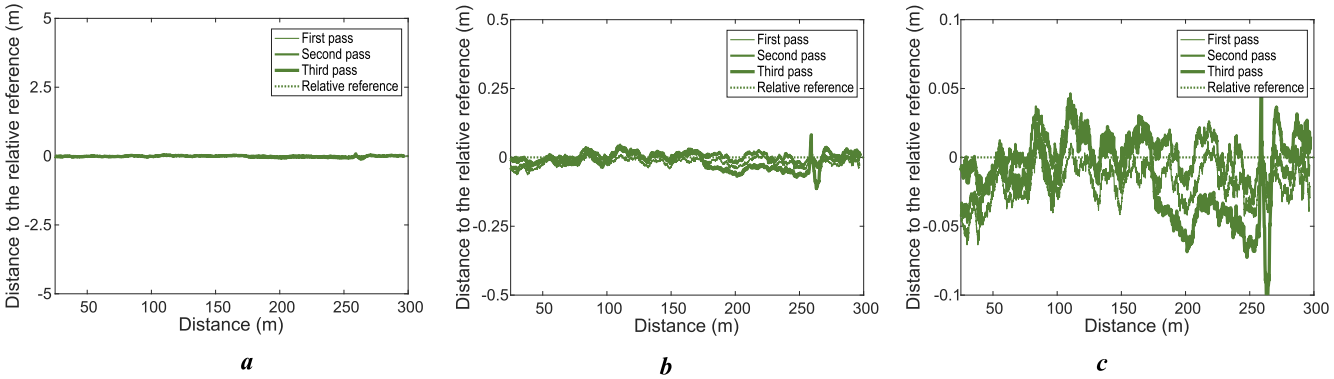


**Fig. C.11.** C11 (Harxon|RTK|42km). Graphs showing the guidance test short-term error of the Harxon TS108PRO receiver with RTK with the reference station in Valladolid, 42 km away from the receiver, with the ordinate axis ranging from: (a) -5 to 5 m, (b) -0.5 to 0.5 m, (c) -0.1 to 0.1 m.

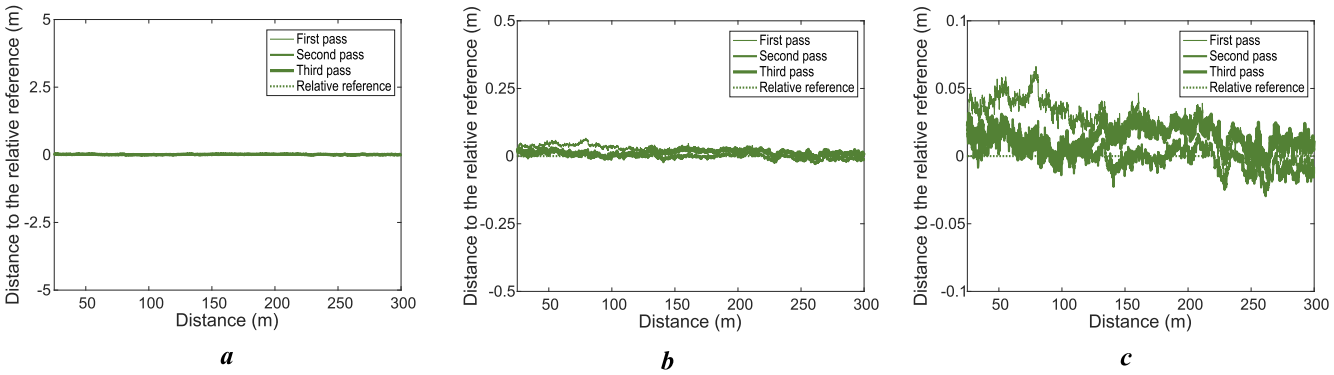


**Fig. C.12.** C12 (Harxon|RTK|14km). Graphs showing the guidance test short-term error of the Harxon TS108PRO receiver with RTK with the reference station in Olmedo, 14 km away from the receiver, with the ordinate axis ranging from: (a) -5 to 5 m, (b) -0.5 to 0.5 m, (c) -0.1 to 0.1 m.

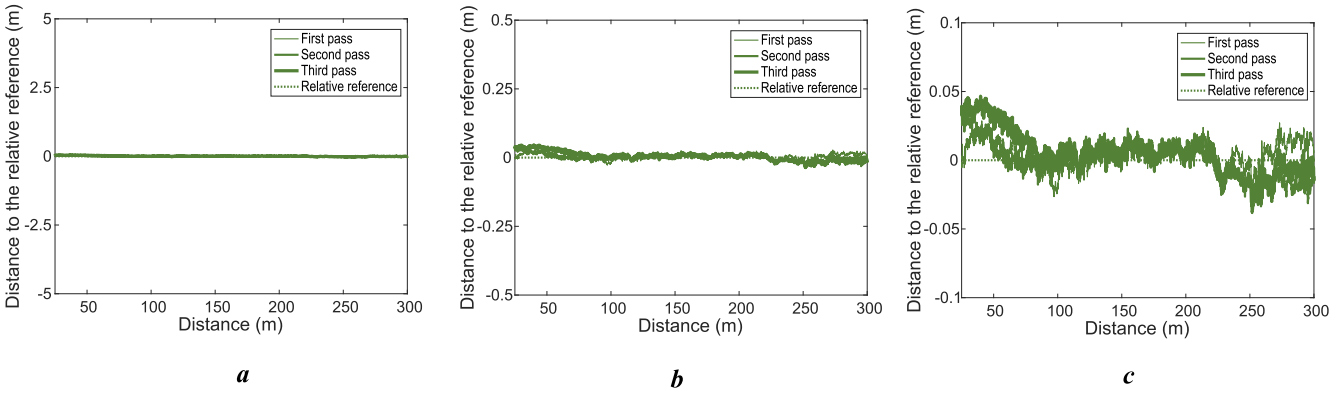


**Fig. C.13.** C13 (Harxon|VRS-NRTK|14,25,42km). Graphs showing the guidance test short-term error of the Harxon TS108PRO receiver with VRS-NRTK with a Virtual Reference Station at the receiver location, with the ordinate axis ranging from: (a) -5 to 5 m, (b) -0.5 to 0.5 m, (c) -0.1 to 0.1 m.

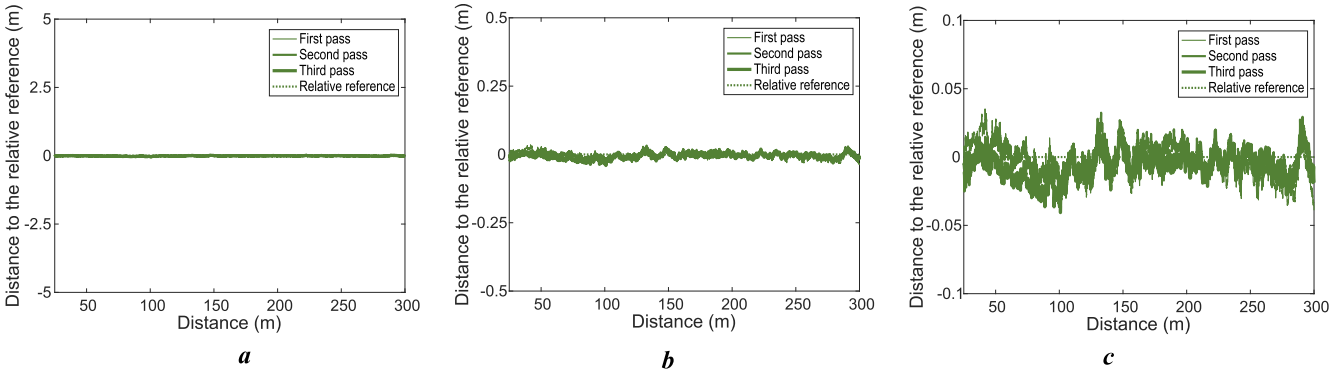


**Fig. C.14.** C14 (Harxon|On-site RTK). Graphs showing the guidance test short-term error of the Harxon TS108PRO receiver with RTK via a base station located a few metres from the receiver, with the ordinate axis ranging from: (a) -5 to 5 m, (b) -0.5 to 0.5 m, (c) -0.1 to 0.1 m.

## Data availability

The dataset acquired in this study is available at DOI: 10.17632/xj3vp2w89y.1.

## References


Alkan, R.M., Erol, S., İlçi, V., Ozulu, M., 2020. Comparative analysis of real-time kinematic and PPP techniques in dynamic environment. Meas. J. Int. Meas. Confed. 163. https://doi.org/10.1016/j.measurement.2020.107995.

Barna, R., Tóth, K., Nagy, M.Z., Solymosi, K., 2020. Technical characteristics of global navigation satellite systems and their role in precision agriculture. J. Agric. Inform. 11. https://doi.org/10.17700/jai.2020.11.1.573.

Carballido, J., Perez-Ruiz, M., Emmi, L., Agüera, J., 2014. Comparison of positional accuracy betweenRTK and RTX GNSS based on the autonomous agricultural vehicles under field conditions. Appl. Eng. Agric. 30, 361–366. https://doi.org/10.13031/aea.30.10342.

China Satellite Navigation Office, 2021. BeiDou Navigation Satellite System Open Service Performance Standard (Version 3.0).

Coyne, P.I., Casey, S.J., Milliken, G.A., 2003. Comparison of Differentially Corrected GPS Sources for Support of Site-Specific Management in Agriculture (Kansas Agricultural Experiment Station Special Publication).

Dabove, P., 2019. The usability of GNSS mass-market receivers for cadastral surveys considering RTK and NRTK techniques. Geod. Geodyn. 10, 282–289. https://doi.org/10.1016/j.geog.2019.04.006.

Dang, X., Yin, X., Zhang, Y., Gao, C., Wu, J., Liu, Y., 2023. Improved medium baseline RTK positioning performance based on BDS/galileo/GPS triple-frequency-only observations. Remote Sens. 15, 5198. https://doi.org/10.3390/rs15215198.

EGNSS Agency, 2025. EGNOS Open Service (OS) Service Definition Document.

EUSPA, 2024. Galileo Open Service Performance Report July-August-September 2024.

Garrido-Carretero, M.S., L.-P. de los de Cobos, M.C., Borque-Arancón, M.J., Ruiz-Armenteros, A.M., Moreno-Guerrero, R., Gil-Cruz, A.J., 2019. Low-cost GNSS receiver in RTK positioning under the standard ISO-17123-8: a feasible option in geomatics. Measurement 137, 168–178. https://doi.org/10.1016/j.measurement.2019.01.045.

Gökdaş, Ö., Özlüdemir, M.T., 2020. A variance model in NRTK-based geodetic positioning as a function of baseline length. Geosciences 10, 262. https://doi.org/10.3390/geosciences10070262.
Grejner-Brzezinska, D.A., Kashani, I., Wielgosz, P., 2005. On accuracy and reliability of instantaneous network RTK as a function of network geometry, station separation, and data processing strategy. GPS Solut. 9, 212–225. https://doi.org/10.1007/s10291-005-0130-1.
Guzman, R., Arino, J., Lopes, C.M., Navarro, R., Graça, J.D., Reyes, M., Barriguinha, A., Braga, R., 2016. Autonomous hybrid gps/reactive navigation of an unmanned ground vehicle for precision viticulture-VINBOT. 62nd German Winegrowers, in.
Hou, P., Zhang, B., Liu, T., 2020. Integer-estimable GLONASS FDMA model as applied to Kalman-filter-based short- to long-baseline RTK positioning. GPS Solut. 24, 93. https://doi.org/10.1007/s10291-020-01008-8.
Jensen, A.B.O., Cannon, M.E., 2000. Performance of Network RTK Using Fixed and Float Ambiguities, in. In: Proceedings of the 2000 National Technical Meeting of The Institute of Navigation. ION (Institute of Navigation), pp. 797–805.
Kadeřábek, J., Shapoval, V., Matějka, P., Kroulík, M., Kumhála, F., 2021. Comparison of four RTK receivers operating in the static and dynamic modes using measurement robotic arm. Sensors 21, 7794. https://doi.org/10.3390/s21237794.
Kaplan, E., Hegarty, C., 2017. Understanding GPS/GNSS: Principles and Applications. Third Edition, Artech.
Karimi, H., 2021. An analysis of satellite visibility and single point positioning with GPS, GLONASS, Galileo, and BeiDou-2/3. Appl. Geomat. 13, 781–791. https://doi.org/10.1007/s12518-021-00391-2.
Keicher, R., Seufert, H., 2000. Automatic guidance for agricultural vehicles in Europe. Comput. Electron. Agric. 25, 169–194. https://doi.org/10.1016/S0168-1699(99)00062-9.
Kowalczyk, W.Z., Hadas, T., 2024. A comparative analysis of the performance of various GNSS positioning concepts dedicated to precision agriculture. Rep. Geod. Geoinformatics 117, 11–20. https://doi.org/10.2478/rgg-2024-0002.
Lange, A.F., Peake, J., 2020. Precision Agriculture, in: Position, Navigation, and Timing Technologies in the 21st Century. Wiley, pp. 1735–1747. Doi: 10.1002/9781119458555.ch56.
Leick, A., Rapoport, L., Tatarnikov, D., 2015. GPS Satellite Surveying. Wiley. https://doi.org/10.1002/9781119018612.
Li, G., Geng, J., Guo, J., Zhou, S., Lin, S., 2018. GPS + Galileo tightly combined RTK positioning for medium-to-long baselines based on partial ambiguity resolution. J. Glob. Position. Syst. 16, 3. https://doi.org/10.1186/s41445-018-0011-x.
Li, S., Zhang, M., Ji, Y., Zhang, Z., Cao, R., Chen, B., Li, H., Yin, Y., 2021. Agricultural machinery GNSS/IMU-integrated navigation based on fuzzy adaptive finite impulse response Kalman filtering algorithm. Comput. Electron. Agric. 191, 106524. https://doi.org/10.1016/j.compag.2021.106524.
Magiera, W., Vārna, I., Mitrofanovs, I., Silabrieds, G., Krawczyk, A., Skorupa, B., Apollo, M., Maciuk, K., 2022. Accuracy of code GNSS receivers under various conditions. Remote Sens. 14. https://doi.org/10.3390/rs14112615.
Mahato, S., Anjan, A., Hosalikar, K., Mohapatra, M., 2024a. High Accuracy Analysis of NavIC Static Kinematic Performance. In: in: 2024 IEEE Space, Aerospace and Defence Conference (SPACE). IEEE, Bangalore, India, pp. 240–243. https://doi.org/10.1109/SPACE63117.2024.10667657.
Mahato, S., Goswami, M., Bose, A., 2025. RTK position solution performance of compact, low-cost GNSS receiver-antenna combinations. Surv. Rev. 57, 301–311. https://doi.org/10.1080/00396265.2024.2429532.
Mahato, S., Goswami, M., Kundu, S., Bose, A., 2024b. Single-baseline long-distance RTK using a CLS GNSS module and open-source software: a case study from India. IETE J. Res. 70, 2905–2916. https://doi.org/10.1080/03772063.2023.2192424.
Mahato, S., Kumar, V., Singh, A., Deshpande, D., Anjan, A., Mitra, A.K., 2024c. NavIC galileo long distance RTK positioning performance. In: Presented at the 2024 IEEE International Conference of Electron Devices Society Kolkata Chapter (EDKCON), IEEE, Kolkata, India, pp. 1–4. https://doi.org/10.1109/EDKCON62339.2024.10870784.
Mahato, S., Shaw, G., Santra, A., Dan, S., Kundu, S., Bose, A., 2020. Low Cost GNSS Receiver RTK Performance in Forest Environment, in: 2020 URSI Regional Conference on Radio Science (URSI-RCRS). IEEE, Varanasi, India, pp. 1–4. Doi: 10.23919/URSIRCRS49211.2020.9113621.
Ministerio de Transporte y Movilidad Sostenible, 2025. Instituto Geográfico Nacional.
Mishra, P., Mahato, S., Ghorui, S., Bose, A., 2024. GIS-GNSS Integrated Cost Efficient Static Monitoring System, in: 2024 International Conference on Emerging Smart Computing and Informatics (ESCI). IEEE, Pune, India, pp. 1–6. Doi: 10.1109/ESCI59607.2024.10497251.
Nguyen, N.V., Cho, W., 2023. Performance evaluation of a typical low-cost multi-frequency multi-GNSS device for positioning and navigation in agriculture—part 2: dynamic testing. AgriEngineering 5, 127–140. https://doi.org/10.3390/agriengineering5010008.
Nguyen, N.V., Cho, W., Hayashi, K., 2021. Performance evaluation of a typical low-cost multi-frequency multi-GNSS device for positioning and navigation in agriculture – Part 1: Static testing. Smart Agric. Technol. 1, 100004. https://doi.org/10.1016/j.atech.2021.100004.
Novatel, 2015. Firmwares GLIDE: superior pass-to-pass performance in applications where relative positioning is critical.
Ntrip-list, 2025. A portal to NTRIP providers around the world [WWW Document]. URL https://ntrip-list.com/.
Pan, L., Pei, G., Yu, W., Zhang, Z., 2022. Assessment of IRNSS-only data processing: availability, single-frequency SPP and short-baseline RTK. Remote Sens. 14, 2462. https://doi.org/10.3390/rs14102462.
Pérez-Ruiz, M., Carballido, J., Agüera, J., Gil, J.A., 2011. Assessing GNSS correction signals for assisted guidance systems in agricultural vehicles. Precis. Agric. 12, 639–652. https://doi.org/10.1007/s11119-010-9211-4.
Radočaj, D., Plaščak, I., Heffer, G., Jurišić, M., 2022. A low-cost global navigation satellite system positioning accuracy assessment method for agricultural machinery. Appl. Sci. 12, 693. https://doi.org/10.3390/app12020693.
Renfro, B.A., Stein, M., Reed, E.B., Morales, J., Villalba, E.J., 2020. An Analysis of Global Positioning System (GPS). Standard Positioning Service Performance for 2019.
Rounsaville, J., Dvorak, J., Stombaugh, T., 2016. Methods for calculating relative cross-track error for ASABE/ISO standard 12188-2 from discrete measurements. Trans. ASABE 59, 1609–1616. https://doi.org/10.13031/trans.59.11902.
Russian Defence Ministry, Roscosmos State Corporation, 2020. GLONASS Open Service Performance Standard [OS PS].
Schaefer, M., Pearson, A., 2021. Accuracy and precision of GNSS in the field, in: GPS and GNSS Technology in Geosciences. Elsevier, pp. 393–414. Doi: 10.1016/B978-0-12-818617-6.00002-0.
Shannon, D.K., Clay, D.E., Kitchen, N.R., 2018. Precision Agriculture Basics. American Society of Agronomy and Soil Science Society of America. https://doi.org/10.2134/precisionagbasics.
Shi, J., Ouyang, C., Huang, Y., Peng, W., 2020. Assessment of BDS-3 global positioning service: ephemeris, SPP, PPP, RTK, and new signal. GPS Solut. 24, 81. https://doi.org/10.1007/s10291-020-00995-y.
Sun, G.O.K., Gibbings, P., 2005. How well does the virtual reference station (VRS) system of GPS base stations perform in comparison to conventional RTK? J. Spat. Sci. 50, 59–73. https://doi.org/10.1080/14498596.2005.9635038.
Sun, H., Slaughter, D.C., Ruiz, M.P., Gliever, C., Upadhyaya, S.K., Smith, R.F., 2010. RTK GPS mapping of transplanted row crops. Comput. Electron. Agric. 71, 32–37. https://doi.org/10.1016/j.compag.2009.11.006.
Sun, Q., Odolinski, R., Xia, J., Foster, J., Falkmer, T., Lee, H., 2017. Validating the efficacy of GPS tracking vehicle movement for driving behaviour assessment. Travel Behav. Soc. 6, 32–43. https://doi.org/10.1016/j.tbs.2016.05.001.
Tabti, L., 2025. Evaluation and comparison of the accuracy and integrity of GPS single-point positioning using EGNOS corrections. J. Indian Soc. Remote Sens. https://doi.org/10.1007/s12524-025-02168-1.
Takai, R., Yang, L., Noguchi, N., 2014. Development of a crawler-type robot tractor using RTK-GPS and IMU. Eng. Agric. Environ. Food 7, 143–147. https://doi.org/10.1016/j.eaef.2014.08.004.
Tu, R., Liu, J., Zhang, R., Zhang, P., Huang, X., Lu, X., 2019. RTK model and positioning performance analysis using Galileo four-frequency observations. Adv. Space Res. 63, 913–926. https://doi.org/10.1016/j.asr.2018.10.011.
Vázquez, J., Lacarra, E., Morán, J., Sánchez, M.A., González, A., Bruzual, J., 2019. EDAS (EGNOS data access service) differential GNSS corrections: a reliable free-of-charge alternative for precision farming in europe. Annu. Navig. 26, 46–58. https://doi.org/10.1515/aon-2019-0005.
Vollath, U., Landau, H., Chen, X., Doucet, K., Pagels, C., 2002. Network RTK Versus Single Base RTK - Understanding the Error Characteristics. Proc, IEEE - PIEEE.
Walter, T., 2020. Satellite-Based Augmentation Systems (SBASs), in: Position, Navigation, and Timing Technologies in the 21st Century. Wiley, pp. 277–306. Doi: 10.1002/9781119458449.ch13.
Wang, E., Song, W., Zhang, Y., Shi, X., Wang, Z., Xu, S., Shu, W., 2022. Evaluation of BDS/GPS multi-frequency RTK positioning performance under different baseline lengths. Remote Sens. 14, 3561. https://doi.org/10.3390/rs14153561.
Wang, J., Yu, X., 2024. Improving the fixed solution by processing the unmodeled errors in GNSS RTK long baseline positioning. GPS Solut. 28, 164. https://doi.org/10.1007/s10291-024-01707-6.
Yin, X., Wang, Y., Chen, Y., Jin, C., Du, J., 2020. Development of autonomous navigation controller for agricultural vehicles. Int. J. Agric. Biol. Eng. 13, 70–76. https://doi.org/10.25165/j.ijabe.20201304.5470.
Zhang, P., Tu, R., Wu, W., Liu, J., Wang, X., Zhang, R., 2020. Initial accuracy and reliability of current BDS-3 precise positioning, velocity estimation, and time transfer (PVT). Adv. Space Res. 65, 1225–1234. https://doi.org/10.1016/j.asr.2019.11.006.
Zhang, Q., Chen, Q., Xu, Z., Zhang, T., Niu, X., 2021. Evaluating the navigation performance of multi-information integration based on low-end inertial sensors for precision agriculture. Precis. Agric. 22, 627–646. https://doi.org/10.1007/s11119-020-09747-x.
Zhang, Z., Pan, L., 2022. Current performance of open position service with almost fully deployed multi-GNSS constellations: GPS, GLONASS, Galileo, BDS-2, and BDS-3. Adv. Space Res. 69, 1994–2019. https://doi.org/10.1016/j.asr.2021.12.002.

## Glossary

*BDSBAS:* BeiDou Satellite-Based Augmentation System
*CDF:* Cumulative Distribution Function
*CEP:* Circular Error Probable
*CPDGPS:* Carrier-Phase Differential GPS
*DGNSS:* Differential Global Navigation Satellite System
*EGNOS:* European Geostationary Navigation Overlay Service
*FKP: Flächen-Korrektur-Parameter* (German for "Area Correction Parameters")
*GGA:* NMEA sentence containing time, position, and fix-quality information
*GLIDE:* Proprietary NovAtel algorithm for smoothing GNSS positions using pseudorange measurements
*GLONASS:* GLObal NAvigation Satellite System
*GNSS:* Global Navigation Satellite System
*GPS:* Global Positioning System
*IGN: Instituto Geográfico Nacional* (Spanish National Geographic Institute)
*IMU:* Inertial Measurement Unit
*iMAX:* Individual Master-Auxiliary Correction
*MAX:* Master-Auxiliary Correction
*NED:* North, East, Down (coordinate system)
*NMEA:* National Marine Electronics Association
*NRTK:* Network Real-Time Kinematic
*NTRIP:* Networked Transport of RTCM via Internet Protocol
*PA:* Precision Agriculture
*PF:* Precision Farming
*PPP:* Precise Point Positioning
*QZSS:* Quasi-Zenith Satellite System
*RMC:* NMEA sentence containing time, date, position, course, and speed information
*RMS:* Root Mean Square
*RTCM:* Radio Technical Commission for Maritime Services
*RTK:* Real-Time Kinematic
*SBAS:* Satellite-Based Augmentation System
*SD:* Standard Deviation
*SDCM:* System for Differential Corrections and Monitoring
*SF: StarFire*, John Deere satellite-based GNSS correction service (includes SF1, SF2, and SF3 accuracy levels)
*SPP:* Single Point Positioning
*VRA:* Variable Rate Application
*VRS:* Virtual Reference Station
*WAAS:* Wide Area Augmentation System
*XTE:* Cross-Track Error